2021•2022

Faculteit Industriële Ingenieurswetenschappen

master in de industriële wetenschappen: chemie

Masterthesis

Evaluating drying kinetics during humidified drying of an active pharmaceutical ingredient using in-line Near Infrared Spectroscopy

PROMOTOR :

Prof. dr. ir. Jozefien DE KEYZER

Prof. dr. ir. Leen BRAEKEN

PROMOTOR :

ir. Steven RUSCH

COPROMOTOR :

Dhr. Brecht DE FRE

PhD. Bart BUEKEN

Martijn Princen

Scriptie ingediend tot het behalen van de graad van master in de industriële wetenschappen: chemie

Gezamenlijke opleiding UHasselt en KU Leuven

2021•2022

Faculteit Industriële Ingenieurswetenschappen

master in de industriële wetenschappen: chemie

Masterthesis

Evaluating drying kinetics during humidified drying of an active pharmaceutical ingredient using in-line Near Infrared Spectroscopy

PROMOTOR :

Prof. dr. ir. Jozefien DE KEYZER

Prof. dr. ir. Leen BRAEKEN

PROMOTOR :

ir. Steven RUSCH

COPROMOTOR :

Dhr. Brecht DE FRE

PhD. Bart BUEKEN

Martijn Princen

Scriptie ingediend tot het behalen van de graad van master in de industriële wetenschappen: chemie

UHASSELT KU LEUVEN

Preface

This master's thesis was a challenging but highly educational experience. In this section, I would like to thank a number of people who helped in achieving a positive result. First of all, I wish to thank my external promoter, ir. Steven Rusch, for his guidance and feedback during the entire process. Secondly, a special thanks to my external co-supervisor Brecht De Fré for the full guidance and educational experience. I have learned a lot about the subject as well as on a personal level. Furthermore, I would like to thank a number of people for the constructive feedback that was provided, such as PhD. Bart Bueken, Prof. Dr. Jozefien De Keyzer, Prof. Dr. Leen Braeken and Prof. Dr. Jeroen Lievens. I would also like to thank the colleagues in the crystallisation technology unit (CTU) at Janssen Pharmaceutica for the positive working atmosphere and for being open to all my questions. Finally, I would like to express my appreciation to my family and friends who have supported me throughout the entire process.

Table of contents

List of tables

List of Figures

Nomenclature

Term	Definition
Active pharmaceutical ingredient (API)	A component of a pharmaceutical product that imparts the intended effects of a drug, also referred to as a drug substance.
Hygroscopicity	The property of a substance indicating that it is capable of adsorbing water.
Water activity (a_w)	The ratio of the vapour pressure of water in a material to the vapour pressure of distilled water under identical conditions.
Process analytical technology (PAT)	A mechanism for analysing pharmaceutical processes by monitoring critical process parameters.
Relative humidity (RH)	The ratio of the partial pressure of water present in the environment to the saturation vapour pressure of water at a specific temperature.
Anisotropic	The property in which differences in measurements appear according to the orientation of the substance.
Attrition	The phenomenon in which particles start to break, also known as particle breakage.
Agglomeration	The phenomenon where small particles form bonds and behave as one larger particle.
Headspace (HS)	The volume of space above a substance in a closed environment, such as a vial or container.
Hysteresis	Phenomenon reflecting the lag of a property between cause and response.

Abstract

Janssen Pharmaceutica develops and produces active pharmaceutical ingredients (API). During the production, the drying process following crystallisation and isolation is of great importance. In this study, the investigated APIs are hydrates and solvates, in which the solvent is bound in the crystal structure. For these compounds, humidified drying is applied, as a specific water content is required. The objective is to understand the drying behaviour of such APIs, more specifically the removal of unwanted, residual solvent and the uptake of water in the crystals up to the desired level. Furthermore, the impact of ambient air on a sample is studied, as it can affect the water content and consequently the analysis results.

Both static and dynamic drying under the influence of a humidified nitrogen flow were used for the drying process. Monitoring was carried out using in-line process analytical technology such as near-infrared spectroscopy (NIR). In addition, other off-line analytical methods such as Karl Fisher titration (KF), gas chromatography (GC) and dynamic vapour sorption (DVS) were used.

With the help of various drying experiments, an insight into the drying behaviour was obtained. A higher relative humidity resulted in faster water uptake and enhanced removal of unwanted solvents, due to the displacement of the solvent molecules from the crystal structure. Furthermore, the influence of the ambient air, directly and in the headspace (HS) of sample vials, proved to be a problem for the analysis of the water content.

Abstract in Dutch

Janssen Pharmaceutica ontwikkelt en produceert actieve farmaceutische ingrediënten (API). Tijdens de productie is het droogproces volgend op kristallisatie en isolatie van groot belang. In deze studie zijn de onderzochte API's hydraten en solvaten, waarbij het solvent gebonden is in de kristalstructuur. Voor deze verbindingen wordt bevochtigd drogen toegepast, omdat een specifiek watergehalte gewenst is. Het doel is inzicht te krijgen in het drooggedrag van een dergelijke API's, meer bepaald de verwijdering van ongewenst, residueel solvent en de opname van water in de kristallen tot op gewenste gehalte. Daarnaast is de invloed van de omgevingslucht op een staal van belang, aangezien dit het watergehalte kan beïnvloeden.

Voor het droogproces werden zowel statische als dynamische droging onder invloed van een bevochtigde stikstofstroom gebruikt. Monitoring werd uitgevoerd met behulp van in-line near-infrared spectroscopie (NIR). Aanvullend werd gebruik gemaakt van andere off-line analysemethoden zoals Karl Fisher titratie (KF), gaschromatografie (GC) en dynamic vapour sorption (DVS).

Met behulp van verschillende droogexperimenten werd inzicht verkregen in het drooggedrag. Een hogere relatieve vochtigheid resulteerde in een snellere wateropname en een verbeterde verwijdering van ongewenste solventen, als gevolg van de verdrijving van de solventmoleculen uit de kristalstructuur. Bovendien bewees de blootstelling met de omgevingslucht, direct en in de headspace van een staal, een probleem te zijn voor de analyse van het watergehalte.

Chapter 1. Introduction

1.1 Context

This study was conducted in cooperation with Janssen Pharmaceutica, an important innovation hub part of Johnson & Johnson. The company is located in Beerse, where the chemical development site is situated, and in Geel, where the production takes place. For this master's thesis, research was conducted in both locations. Janssen Pharmaceutica is specialised in the research, development, and production of pharmaceuticals and the active pharmaceutical ingredients (API) therein. An API is a component of a pharmaceutical product that imparts the intended effects of a drug, therefore also called a drug substance. Some pharmaceuticals have multiple APIs to treat different symptoms or function in various ways [1]. Following their production by (bio)chemical means, APIs are mixed with excipients to become a drug product (medicine as commonly known).

APIs may occur in various solid forms, such as crystalline polymorphs, pseudopolymorphs, amorphous solids, co-crystals, and salts. These solid forms often exhibit different properties, for instance in terms of their hygroscopicity, stability, dissolution rate, density, melting point, etc. all of which are important in the development of a pharmaceutical product [2]–[5]. This study focuses on the pseudopolymorphs, namely the hydrates and solvates. Many active pharmaceutical ingredients are hygroscopic and readily exchange water molecules with the environment [6]. If these water molecules are included in the crystal lattice of an API, it is considered a pseudopolymorph, more precisely a hydrate (solvate in the case of solvent molecules). Compared to similar anhydrates, they exhibit a different structure, as the presence of water or solvent molecules modifies the complex H-bonding network in the solid state [4]. Hydrates are commonly categorised into isolated (stoichiometric) hydrates, channel hydrates, and ion-assisted hydrates (the same terminology applies for solvates). Channel hydrates generally exhibit lower thermal stability as water molecules can easily diffuse along the channel axis [7].

If the stable form of an API is a hydrate, it is important that this form is preserved during synthesis, isolation, drying and further processing of the compound. For this purpose, process analytical technology (PAT) can be used to analyse various properties of the hydrate in a continuous way. Examples of these PAT include near-infrared spectroscopy (NIR) and Raman spectroscopy. Also, other analytical techniques such as dynamic vapour sorption (DVS), Powder X-ray diffraction analysis (PXRD), thermogravimetric analysis (TGA), etc. are widely used in this industry [3], [5], [8]–[16].

Several parameters influence the formation and/or retention of the hydrate. The most important parameters are temperature, pressure, relative humidity, and the solvent [6]. Relative humidity (RH) is defined as the percentage of saturated moisture at a given temperature. The stability of the hydrate is important during the entire production of the API, from crystallisation to the final product. However, the focus of this study is on the drying process and more specifically on drying using a humidifier.

1.2 Problem Definition / Research Question

In the pharmaceutical industry, it is important for an API to remain chemically stable and to retain the desired polymorphic form during the crystallisation process and the downstream processing of the compound. For a hydrate, it is therefore important to maintain a certain water content and avoid dehydration. Moreover, a high water content could also be undesirable as it affects the powder flowability and density of the product, creating several challenges. First, the API studied in this research (compound A) is a chlorohydrate salt. Therefore, this component is atypical and will behave differently from "normal" hydrates.

A second challenge arises from the fact that a powder, unlike a liquid, is anisotropic. This means that the properties depend on the orientation of the product, which poses a problem when using NIR as a means to track changes in the solid. Measured spectra from different angles of the powder consequently show varying data. The application of an online NIR measurement is therefore interesting. Since the probe in the lab setup is mounted through the wall of the oven, directed onto the sample, and static drying takes place, the angle on the powder will hardly change.

A next challenge occurs after the washing step following filtration or centrifugation of the crystallized solid. For compound A, washing was done with Methanol (MeOH) or isopropyl alcohol (IPA) as the final washing solvent. After drying the compound without humidifying, MeOH or IPA is still present in the API. However, for each solvent, a maximum amount of residual solvent is allowed in a final product (MeOH: 3000 ppm, IPA: 5000 ppm). Since thermal stability is important for compound A (maximum of 50°C), it is required to use humidified drying. The presence of water ensures an exchange of the undesired residual solvent with water molecules.

A final problem, related to the development site in Beerse, is the influence of headspace on the hydrate during transport and storage. Depending on the water activity of the compound, water will migrate to or from the environment or headspace resulting in product adsorption or desorption. When a sample is prepared with a large headspace above it, the hydrate has the possibility to exchange moisture with the air in this headspace. However, when a sample is prepared without headspace, this possibility does not exist, and the moisture content of the hydrate cannot change.

1.3 Research Objectives

The objectives can be divided into two groups; the first group consists of the objectives of the development site in Beerse, and the second group includes the objectives of the production site in Geel. In Beerse, an API under development is used, namely compound A, a hydrate of a chlorohydrate salt. For the humidified drying process, an oven in combination with a humidifier is used. This setup has not been used before within this research group, and therefore the first objective is to characterise and optimise this combination. A second objective is the determination of the drying behaviour of compound A at different relative humidities. This also includes a stress test to determine the limits at what drying conditions the hydrate retains the required properties and quality of crystals, which is important for the development and production of an API. This can be achieved by using PAT and other analytical tools, such as NIR, XRD, DVS, etc. Once the drying behaviour is obtained, it can be compared with other hydrates (e.g. with a channel hydrate).

The next objective is to remove and analyse the washing solvent using humidified drying. A final API must not contain any MeOH residue. Furthermore, the influence of different relative humidities on the MeOH content needs to be analysed. As a final objective for the research in Beerse, the significance of the influence of the headspace on a sample during transport and storage is to be evaluated.

For the research in Geel, the production, more specifically the humidified drying of compound B, a channel hydrate, are to be analysed. During this production, a large number of data have already been collected which have not yet been analysed. This process data provides a great amount of information regarding the humidified drying process on a production scale and will be used in comparison with the observations obtained from the drying experiments on a laboratory scale.

Chapter 2. Literature Survey

This thesis focuses on the humidified drying process of pharmaceutical hydrates and solvates, and the importance of determining the characteristics and behaviour of these APIs. To fully understand the drying process, and the characterisation methods involved, a preliminary literature study is required. In section 2.1, the concept of an API and the production process of these APIs is introduced. Furthermore, this section zooms in on pseudopolymorphs, namely the hydrates and the solvates. Regarding the production process of APIs, this study mainly examines the drying unit operation, more specifically the humidification drying. This process and the negative phenomena that can occur should therefore be well understood and are explained in section 2.2. In the humidified drying process, the term relative humidity is highly important. Therefore, it is required to understand this term and the influences of ambient conditions, such as temperature and pressure, on this humidity. This is discussed in depth in section 2.2. Finally, understanding the behaviour and drying kinetics of an API during such a drying process is essential. Different characterisation methods are possible to achieve this. In section 2.3 several PAT and analytical methods are discussed and explained.

2.1 Active pharmaceutical ingredient

An active pharmaceutical ingredient of a pharmaceutical product, also called a drug substance, is the component which imparts the intended effects of a drug. Following the production of a final API, it is mixed with excipients to become a drug product (medicine as commonly known). The excipients used vary depending on the API and the type of drug product (tablet, ointment, capsule, etc). Some pharmaceuticals have multiple APIs to treat different symptoms or function in various ways [1], [2].

2.1.1 production process

The production of an API consists of several successive processes. The first process is the reaction, which involves several stages. The products formed during these stages are referred to as intermediates, and eventually, the final API is produced. Once the final API is achieved, a crystallisation step is (usually) required. In the pharmaceutical industry, two types of crystallisations are generally used, one based on a temperature reduction and the other based on an anti-solvent addition. The following step is the separation and purification, followed by a washing of the filter cake. The washing step can have various purposes. First, the API can contain impurities such as salts which have to be removed, but the washing step can also be implemented as a solvent exchange. After washing, an API has to be dried. In the drying process, a division can be made between static and dynamic drying. This process is the focus of this study and will be discussed in more detail in a later section. After the drying process, other downstream processes can be carried out such as milling of the API crystals using techniques such as high shear milling or jet milling. A systematic representation of the production process is shown in Figure 1.

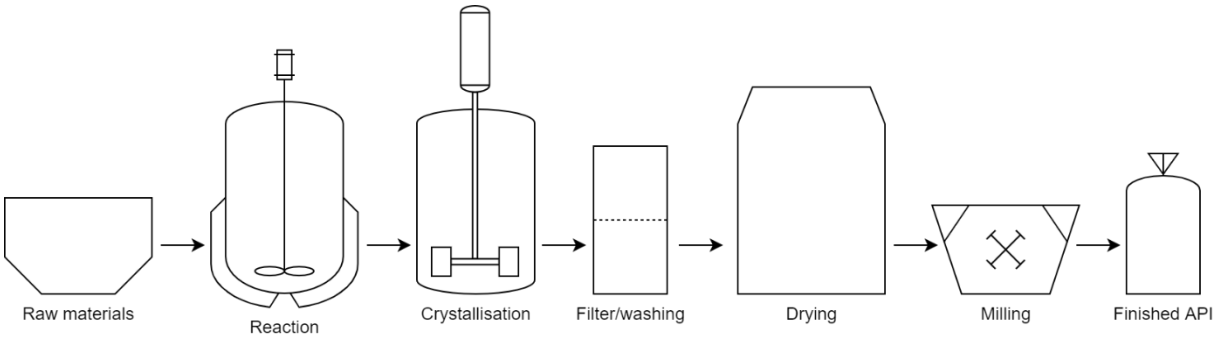

Figure 1. Production process API

2.1.2 Polymorphism

APIs may occur in various solid forms, such as crystalline polymorphs, pseudopolymorphs, amorphous solids, co-crystals, and salts. The term polymorphism refers to crystalline solids which, besides having the same chemical compositions, differ in crystal packing, lattice energy and the molecular arrangement in the crystal lattice [3], [5], [17]. This molecular arrangement is controlled by temperature, relative humidity, pressure, but also the solvent used during crystallisation and further downstream processes [2], [4], [10]. Polymorphic solids may differ in their physicochemical properties such as hygroscopicity, the flowability of the powder, melting point, density, tabletability, solubility, etc [3]–[5], [10], [18]. It is therefore important that the crystal structure and the different polymorphs are known before the development and production of an API [10], [19]. The complexity, however, is that these boundaries differ for each API, and therefore, thorough research is needed to obtain and maintain a desired API form during complete production [8]. The solvents used during crystallisation or further downstream processes can be incorporated into the crystal structure of the API. This phenomenon is called pseudopolymorphism [3]. If this incorporated solvent is water, a hydrate is formed, otherwise, it is referred to as a solvate. Different polymorphic forms can be analysed using Powder X-ray diffraction analysis (PXRD) [3], [5], [8], [10], [20].

2.1.2.1 Hydrates

For certain APIs, hydrates are the preferred form as the presence of other solvents can have toxic and negative effects on the API and its effectiveness, which is certainly a problem in the pharmaceutical industry [3]. The water incorporated in the active pharmaceutical ingredient may have different roles. These molecules can form hydrogen bonds with other water molecules and with functional groups of the API [6].

Hydrates can be divided into three categories according to their water topology and structure [7]. First, the isolated site hydrates. In this category, the water molecules are isolated by intervening drug molecules and thus not in contact with the other water molecules. A second category is the channel hydrates. Here the water molecules lie next to each other parallel to the axis of the crystal lattice. In these so-called channels, the water molecules can interact through weak interactions. Channel hydrates generally exhibit lower thermal stability as the water molecules are able to diffuse along the channel axis. The last category is the metal ion-associated hydrates. Here the water molecules are bound and coordinated with metal ions [3], [5], [7]. Hydrates can also be subdivided into stoichiometric and non-stoichiometric hydrates according to the size of the channels and the extent of hydrogen bonding. The difference between the two is the fact that stoichiometric hydrates

contain a fixed water to API ratio and non-stoichiometric hydrates have variable water content. As a result, water molecules are generally more strongly bound in stoichiometric hydrates [3].

Approximately one-third of the APIs can form hydrates. Due to the physicochemical properties of water, the molecule can readily fill structural voids in the crystal structures of these APIs and, with the help of hydrogen bonds, link the drug molecules to form a stable crystal structure [5], [21]. Determining the most stable form is important for the development of the API. The hydrate form is influenced by a variety of conditions, such as temperature, pressure, and relative humidity. For instance, a transition from a hydrate to an anhydrate form can take place during several development and production processes [3], [5], [8]. As previously mentioned, it is therefore important to have insight into the polymorphism and pseudopolymorphism of an API.

2.1.2.2 Solvates

As mentioned before, besides hydrates there exists another type of pseudopolymorph, the solvates. In solvates, solvate molecules are incorporated into the crystal lattice during crystallisation or further downstream processes [3], [5], [21]. Hydrates are in fact a subclass of solvates in which the solvent is water. Solvates also exist in either stoichiometric or non-stoichiometric proportions to the drug molecules [5].

The fact that hydrates and solvates may behave similarly allows both water and solvent molecules to be present in the crystal structure. The ratio of this is determined by various factors such as the affinity of the API, the available molecules in the environment, the available space in the crystal lattice, etc. In the study by Lamberto et al. 2021, humidified nitrogen was used during the drying process to enhance solvent removal and solvent displacement with water [22]. In addition to this phenomenon, solvates can also release the solvate molecules from the crystal lattice, known as desolvation. Desolvated solvates maintain the crystal structure of the solvates from which they are formed. These desolvated solvates are complicated to characterise since analytical methods suggest that they are anhydrous crystal forms and therefore unsolvated materials [5], [23].

2.2 Drying

This study focuses on the drying process of the API, an important unit operation in the pharmaceutical industry. As previously described, an API can occur in different polymorphs and pseudopolymorphs. The main interest will be in the pseudopolymorphs, being the hydrates and solvates. Knowing the drying mechanism of a particular API is essential for obtaining a consistent drug substance [18]. The properties of an API important for achieving an optimal drying process are shown in Figure 2.

Before the drying process can be studied, several aspects have to be understood. First, the difference between free and bound water present in a hydrate. Free water is defined as water unbound in the crystal structure of the API, usually obtained from crystallisation, and washing of the product. Bound water, or hydrate water, refers to water experiencing a mass transfer limitation. For example, water incorporated into the crystal lattice of the hydrate, water bound to the crystal surface or water bound in small pores and cracks [11], [15], [22]. In general, during a drying process, the free water is removed first, as no additional energy is required to detach from the crystal structure. This period is referred to as the constant rate period. For bound water, however, additional energy is necessary, making the process slower and more difficult, known as the falling rate period [20], [22]. Figure 3 represents a typical drying curve with the constant and the falling rate period. Next, the mechanism of dehydration must be understood. Dehydration involves three stages. Firstly, bound water has to overcome an energy barrier which allows water to behave as mobile in the crystal structure. Next,

the water molecules diffuse out of the crystal lattice and, finally, the released water is removed with a carrier gas [8], [17], [24].

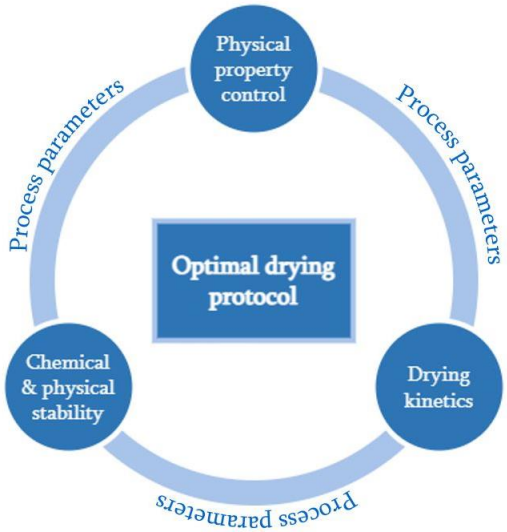

Figure 2. Important properties of the API for an optimum drying protocol [20, p. 421]

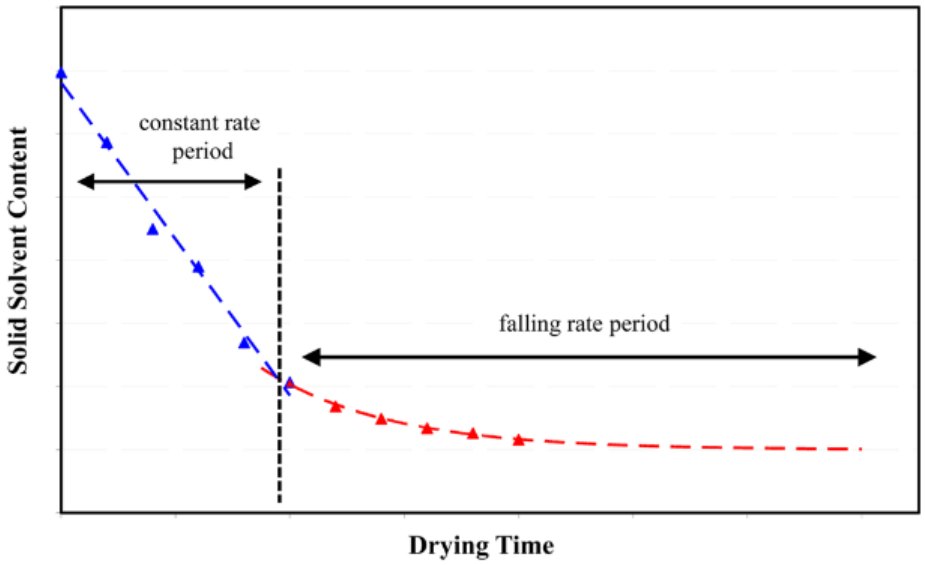

Figure 3. Typical drying curve [20, p. 423]

2.2.1 Drying techniques

There are numerous possibilities and methods for the drying process in the pharmaceutical industry. Various parameters are of importance in such a drying process. First of all, the temperature and pressure at which drying takes place. The temperature is determined by the solvent that has to be removed and the thermal stability of the API. Most APIs have a thermal stability below 80°C, and therefore drying generally takes place at a temperature lower than 80°C. In addition, a reduced pressure (vacuum) is frequently used. A reduced pressure generally results in a reduction in the boiling temperature of the solvents to be removed. Due to thermal stability, lower pressure is often

used in order to obtain the same drying efficiency at a lower temperature. Subsequently, a nitrogen flow is often applied to remove the released solvent vapours. The flow rate of this nitrogen stream is also an important parameter. Generally speaking, at a higher flow rate, the solvent vapours are removed faster.

This study focuses on batch dryers. First of all, a distinction can be made between two groups, namely static and dynamic drying. Static drying, as the name implies, does not involve any agitating of the API. An example of static drying is vacuum tray drying, shown in Figure 4. This type of dryer uses contact drying at reduced pressure and is a relatively inexpensive type of dryer. The advantage of static dryers is that nearly every form of solid can be dried without mechanical damage, however, the drying times are relatively long [25]. In dynamic or agitated drying, on the other hand, the API is agitated during the drying process. This generally results in better contact, allowing homogeneous drying. An example of dynamic drying is an agitated vacuum dryer, shown in Figure 5. This type of dryer also works at reduced pressure but is equipped with an agitator. The disadvantage, however, is the effect of shear stress and hydrostatic pressure, which can result in particle breakage [20].

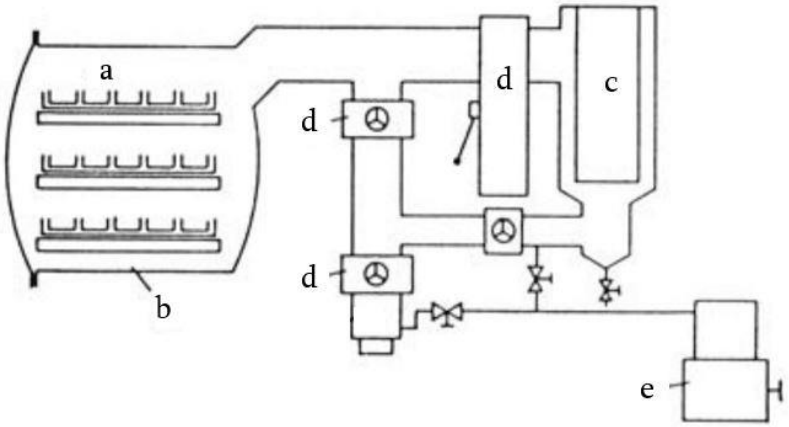

Figure 4. Schematic of a vacuum tray dryer; (a) heated trays; (b) oven; (c) condenser; (d) valve; (e) pump [26, p. 613]

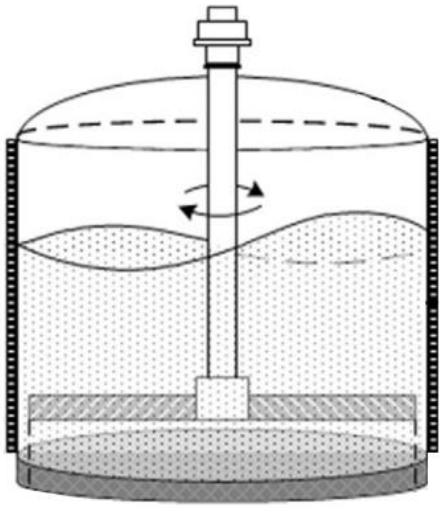

Figure 5. Schematic of an agitated vacuum dryer [27, p. 147]

In case it is desired for the development and production of an API to preserve the API as a crystalline hydrate, a humidified nitrogen flow can be applied during the drying process. In this way, the relative humidity within the dryer can be regulated and a certain water content can be achieved. The exchange of water between the API and the environment differs for each hydrate. The relation of the relative humidity to the water content possessed by the API is described in a vapour sorption isotherm. More detail on obtaining such an isotherm is discussed in section 2.3.1. In the pharmaceutical industry, a humidified nitrogen flow is also used to extract undesired solvents from the API more effectively [22]. Solvents are undesirable in a final product, therefore it is essential they are removed during the drying process. The amount of residual solvent allowed to be present in a final API is fixed. For each solvent, this value is stated in the international council for harmonisation of technical requirements for pharmaceuticals for human use (ICH) guidelines [28]. For solvates, where the solvent is bound into the crystal lattice, the low concentrations of solvent can be rather difficult to remove during a conventional drying process. A humidified drying process could solve this problem. The water molecules, present during the drying process, are able to replace the solvent molecules in the crystal lattice, resulting in the formation of a hydrate (mainly applies to channel solvates only) [22]. As opposed to solvates, hydrates are accepted as final API since water has no toxic effects on the human body. This phenomenon is not observed in all solvates. Firstly, it mainly occurs with channel solvates. Here, the channels ensure that the solvent molecules become more mobile along the axis of the channels, making an exchange with water easier. Secondly, the rate at which this phenomenon takes place, and whether it in fact does happen, depends on the relation between the solvent and the API. If the API shows more affinity towards the solvent than towards water, the exchange will not occur. Especially not for the last strongly bound solvent molecules.

When humidified drying is applied, there is a major contrast between static and dynamic drying. With static drying, the cake resistance will be of great importance. The cake resistance describes the resistance a liquid or gas must overcome to diffuse through a medium. This resistance increases with the thickness of the cake. Therefore, an API at the bottom of the cake experiences much less influence from the humidified nitrogen as here the resistance is the greatest, as shown in Figure 6. In dynamic drying, however, this does not pose a problem. By stirring during the drying process, all API crystals are equally exposed to the humidified nitrogen, resulting in a much more rapid and efficient exchange of water molecules.

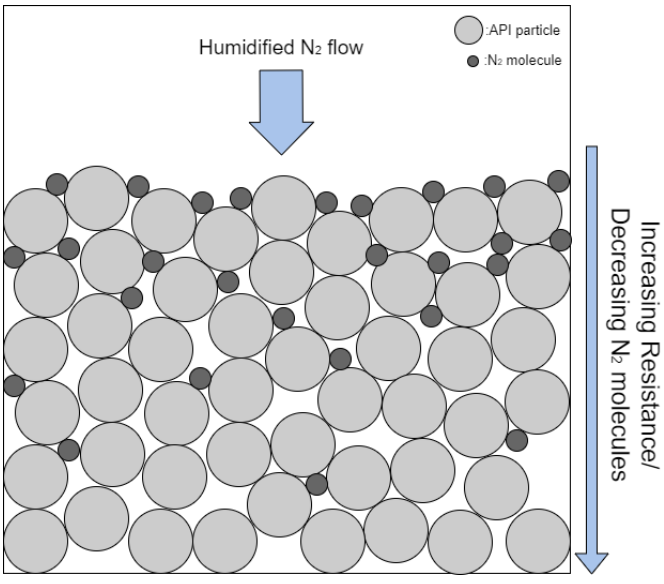

Figure 6. Schematic of influence cake resistance and cake thickness

2.2.1.1 Particle breakage & agglomeration

As mentioned earlier, a distinction is made between static and agitated drying. Agitated drying is mainly preferred in the pharma industry due to lower drying times and better homogeneity during drying. Agitation during drying ensures better heat and mass transfer rates as the particles are redistributed continuously. In general, drying is rapid at the surface and the side of the dryer due to the carrier gas at the surface and the jacket heat at the side of the dryer [20], [29].

However, dynamic drying also has disadvantages. Primarily, two phenomena can occur, namely particle degradation and agglomeration [20], [30]. particle attrition or breakage may occur during agitated drying due to the force applied from particle to particle, from agitator to particle or from the wall to the particle. Figure 7 shows the influence of the agitator on the particles. Here it is visible that the crystal particles are broken, and therefore smaller, by being forced under the agitator. The occurrence of attrition results in a decrease in the overall particle size and an increase in the particle size distribution (PSD), which can cause the final product not to meet the quality requirements [20], [31]. Previous studies show that attrition is higher for the wet cake compared to the dry cake, due to the mobility of the particles and the higher force required for agitation [32], [33]. The unbound water molecules present in a wet cake act as an adhesive between the different particles. As a result, the force required for agitation is higher, and consequently also the force exerted on the crystals. A dry cake has a higher powder flowability, making the powder flow easier over each other and causing less resistance and thus less particle breakage. Papageorgiou et al. 2020 stated that it depends on the API and the solvent. In some cases, attrition is higher for the dry cake compared to the wet cake and the solvent behaves as a lubricant. In other cases, less attrition is observed when the solvent content is reduced [33]. Besides agitation, dehydration and desolvation of the crystalline form result in destabilisation and a reduction in particle size according to Lamberto et al. 2011 [32].

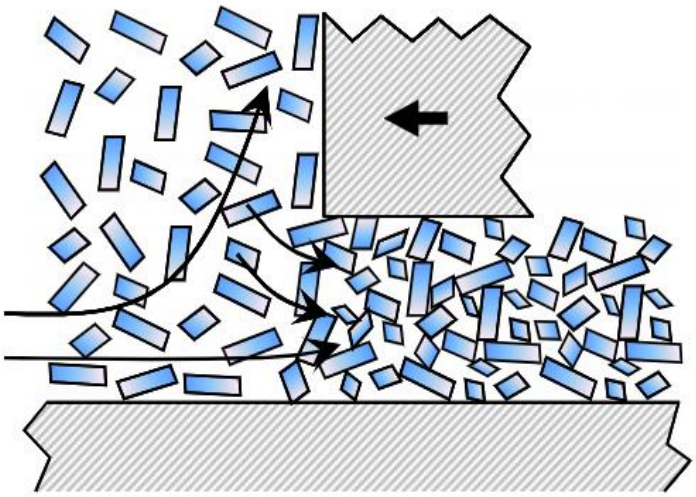

Figure 7. Schematic of influence agitator blade on the particles during dynamic drying [32, p. 3869]

Agglomeration is the phenomenon where small particles, also referred to as fines, form bonds and behave as one larger particle [31]. Therefore, agglomeration is related to attrition. The more particle breakage, the more fines present to form agglomerates. In addition to the size of the particles, the shape also affects the formation of agglomerates. API crystals with a needle shape, shown in Figure 8, can agglomerate the easiest. Agglomeration can also be related to the fact that the wet cake can

still contain some API in solution. During drying, this will crystallise and can form bridges and act as a glue between the particles. According to several studies, agglomeration is, like attrition, dominant at the beginning of the drying process and thus at the wet cake [20], [33]. Agglomeration adversely affects the quality of the API, the PSD, and the cycle times. They can also hinder the removal of the product from the equipment [31]. Therefore, the mechanical properties of the material must be understood during the drying process. Insufficient knowledge may lead to undesired breakage, long drying times, and loss of material. It is not always possible to predict the behaviour of the component in production with a pilot plant in a lab. The type of dryer used usually depends on the availability of the installation and the stage of development of the API [20], [29], [32]. If a dynamic agitated dryer is used, more attrition and agglomeration will be encountered compared to using a static dryer. According to the study by Zhang et al. 2014, in addition to minimising stirring during drying, another solvent system can be opted for the final washing step after crystallisation to minimize attrition, due to the viscosity of the solvent. A lower viscosity of the solvent results in a lower force needed for agitation. This is caused by lower surface tension at low viscosity, resulting in weaker cohesive forces in the liquid [29].

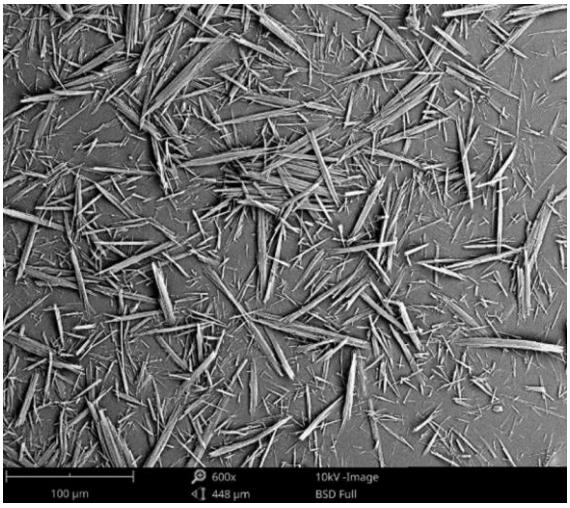

Figure 8. SEM result of needle-shaped crystals (600x)

2.2.2 Relative humidity

Multiple factors influence the water behaviour in hydrates. The most important factor is relative humidity [8], [22]. Humidity can be defined as absolute and relative humidity. Absolute humidity refers to the amount of water present in the environment at a specific temperature. Relative humidity, on the other hand, is the amount of water present in relation to the total possible amount of water. So relative humidity is obtained by the ratio of the partial pressure of water present in the environment (p_{water}) to the saturation vapour pressure of water at a specific temperature (p_{sat}), as shown in equation 1.

$$\% RH = \frac{p_{water}}{p_{sat}(T)} x\ 100 \qquad (1)$$

The relative humidity is strongly dependent on temperature and pressure. An increase in temperature, without the addition or evaporation of water, results in a decrease in relative humidity. This can be explained by the fact that warm air is able to contain more water as shown in Figure 9. Therefore, the saturation vapour pressure of water increases causing the relative humidity to decrease. The relationship between temperature and humidity is described in a Mollier diagram, shown in Figure 10. This diagram contains the absolute humidity (x-axis), the temperature (y-axis), the relative humidity (blue) and the enthalpy (red). The figure shows the effect of a temperature increase (from 0 to 1). In this example, a temperature increase of 10°C starting from 20°C and a RH of 50% results in a relative humidity of approximately 28%.

The impact of pressure is explained based on changes in partial pressure of water. At a constant temperature, an increase in pressure can be considered a volume reduction. Consequently, there is less free space for water molecules, so the partial pressure of water increases. This results in an increase of the relative humidity. In a vacuum, the opposite occurs and the relative humidity decreases.

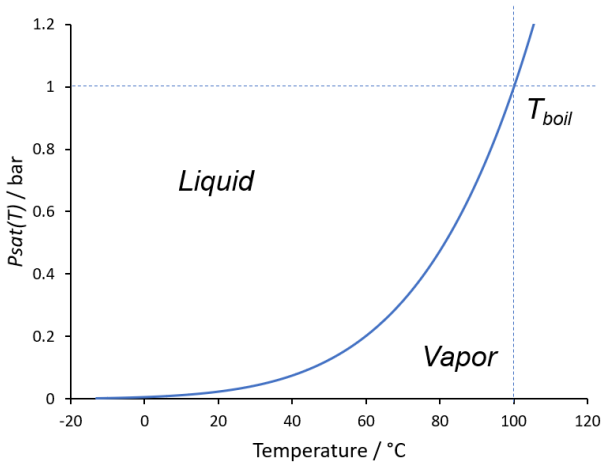

Figure 9. Influence temperature on equilibrium vapour pressure

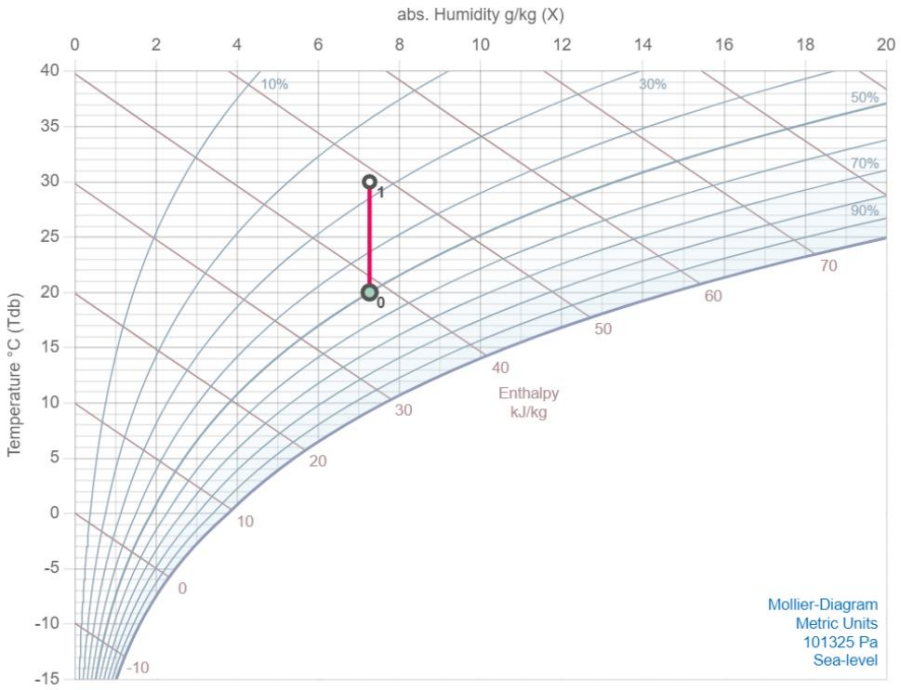

Figure 10. Mollier diagram [34, p. 1]

During the production of hydrates and solvates, a specific relative humidity is very important. This humidity can be obtained by various techniques. During the drying process of an API, a humidifier is generally used. During this technique, a dry flow of inert gas, usually N_2, is directed through the humidifier. In the humidifier used in this study, the dry flow is humidified by the transfer of water molecules through membrane tubes. The obtained humidified nitrogen flow is subsequently used during the drying process [22].

A specific humidity can also be obtained with salt solutions. Salt solutions are mixtures of distilled water and pure salt. The salt retains a certain amount of water molecules making the atmosphere not completely saturated with water. Different salts are used to achieve different humidities since each salt interferes with water differently. This technique is often used for calibration purposes [6], [35]. Table 1 shows the equilibrium relative humidities of various saturated salt solutions. For example, a relative humidity of 75.1% is obtained when using a saturated NaCl solution at 30°C.

Table 1. Relative humidities of different saturated salt solutions

Salt solution	Temperature (°C)		
	30	40	50
LiCl (Lithium chloride)	0.113	0.112	0.111
$MgCl_26H_2O$ (Magnesium chloride)	0.324	0.316	0.305
K_2CO_3 (Potassium carbonate)	0.431	0.433	0.427
$Mg(NO_3)_2$ (Magnesium nitrate)	0.514	0.484	0.454
NaCl (Sodium chloride)	0.751	0.747	0.743

2.2.3 Water activity

The presence of water in the ambient air, thus the relative humidity, is not an indication that an API will form a hydrate. Some APIs, despite the fact they can dissolve in water, are unable to form a hydrate. The water activity (a_w) of a substance is the property which determines the behaviour of this substance towards water and whether a hydrate can be formed [5]. The water activity of a certain substance refers to the amount of available water (the chemical potential of water) and is determined by the ratio of the vapour pressure of water in a material to the vapour pressure of distilled water under equal conditions, with a value between 0 and 1. If this substance is air, there is a close relationship between water activity and relative humidity. Both refer to the amount of water available. For example, air with a relative humidity of 40% has a water activity of 0.4.

Water activity is also an interesting property in the pharmaceutical industry. The water activity reflects the hygroscopicity of a hydrate. A hydrate with a low water activity contains a low amount of water and thus a lot of available binding sites and will therefore readily adsorb water, making it highly hygroscopic. If the ambient air has a larger water activity, there is more water available, and water can therefore be exchanged with the hydrate. This phenomenon is illustrated in Figure 11. Water migrates from a substance with a high water activity to a substance with low water activity. The rate at which this occurs depends, among other things, on the extent of the difference in water activity of both substances.

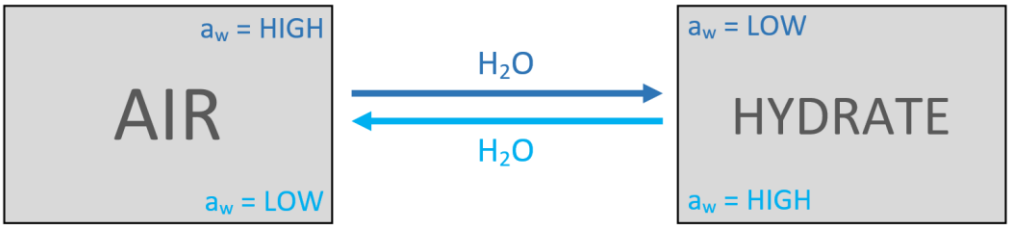

Figure 11. Schematic of water exchange between substance and ambient air

2.2.3.1 Headspace

The headspace of a sample consists of the surrounding air at the time the container is closed and therefore has the same water activity as the surrounding air of that time. As mentioned earlier, a substance can be impacted by the ambient air if the water activities differ and therefore water can be exchanged from high to low water activity. This makes it important to isolate a substance that is expected to exchange water with the ambient air. Once the sample has been sealed off, however, it may still be influenced by the headspace.

The headspace may interact in a similar way with the sample as the ambient air. However, the number of available water molecules will change more rapidly, and an equilibrium will be reached more quickly between the sample and the headspace. Assume that the water activity of the headspace is higher than that of the sample. The sample will behave in a hygroscopic manner and water molecules will be exchanged from the headspace to the sample until an equilibrium is reached and a similar water activity is obtained. The water activity at which equilibrium is reached depends, among other things, on the ratio of the headspace to the sample. In a small headspace, as shown in Figure 12 (c), the number of water molecules that can be exchanged decreases rapidly, resulting in an equilibrium closer to the water activity of the sample. In contrast, the ambient air can be considered as an infinitely large headspace, as shown in Figure 12 (a), thus the sample has a small

influence on the number of available water molecules that can be exchanged. In this case, an equilibrium is reached closer to the water activity of the ambient air. For the analysis of hydrates that can exchange water rapidly, it is therefore important that the sample is analysed accurately. This phenomenon has not yet been demonstrated in the literature and will be examined in this study.

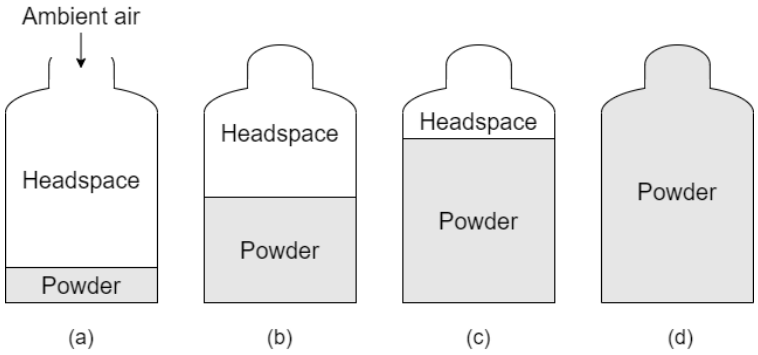

Figure 12. Different headspace to sample ratio in a container; (a) infinite headspace (ambient air); (b) equal ratio of headspace and powder; (c) small headspace; (d) no headspace

2.3 Characterisation methods

The use of process analytical tools during the drying process provides a number of valuable benefits. Firstly, the drying time is reduced as it becomes apparent when a specific solvent content is reached. This is also linked to the second benefit, which is the reduction or elimination of over-drying. Finally, energy consumption is reduced which also results in lower overall costs [36]. In addition to PAT, during the drying process samples are usually taken on which different characterisation methods are applied. These will also aid the development and performance of the drying process.

2.3.1 Dynamic Vapour Sorption

Water vapour sorption analysis is a technique for analysing the water adsorption and desorption behaviour of a substance. The result is a sorption isotherm that allows an understanding of the rate and way water is incorporated and the influence on the solid form [3], [35]. Dynamic vapour sorption analyses the difference in mass of a sample by applying a flow with a specific water activity over the sample. This difference in mass is correlated to the water uptake and release of the sample and is measured with an ultra-sensitive microbalance. Important for this analysis is to reach an equilibrium of the water content within the sample at a certain relative humidity. The advantage of the DVS is that small quantities of samples can be examined, which minimises the time to reach equilibrium. A vapour sorption analyser is also capable of determining the instantaneous water activity of a sample. For this purpose, an equilibrium is reached between the water activity in the headspace above the sample and the water activity of the sample itself. The detector analyses the a_w of the headspace.

At relatively low relative humidities, the water adsorption rate is in general the highest. Hydrates in this range theoretically contain no water and are therefore strongly hygroscopic. When water molecules are introduced, they are rapidly adsorbed by the hydrate. This is visible in the sorption isotherm as a steep slope, indicating that the first interactions with water molecules are the strongest. These water molecules not just fill voids, but also form strong interactions with the crystal

lattice. For this reason, these water molecules are also the hardest to extract. As more water molecules are adsorbed, they behave more mobile and are less bound in the crystal structure. This behaviour cannot be generalised for all hydrates, as each hydrate exhibits a unique behaviour, but it is frequently seen with several APIs in the pharmaceutical industry [3], [4], [22], [24].

2.3.1.1 Hysteresis

An important phenomenon that frequently occurs in sorption isotherms is a hysteresis [3], [6], [13]. A hysteresis represents the difference in adsorption and desorption behaviour resulting in different curves. There are various reasons why hysteresis might appear. A first reason has already been mentioned above, namely when the sample did not reach equilibrium at a specific relative humidity. Another common cause is if the diffusion of water molecules out of the crystal lattice is more difficult than the diffusion into the crystal structure. Because the water molecules form strong interactions with the crystal lattice when they are adsorbed, the energy and force necessary to get the water molecules out of the crystal structure are much higher [3]. A next possibility for hysteresis is that pore size varies during adsorption and desorption, also referred to as capillary condensation [6]. Another possible cause is that polymers, peptides, and proteins may undergo a transition to amorphous materials as a result of water adsorption [6], [13], [18], [24]. A final reason occurs in stoichiometric hydrates. With this type of hydrate, the energy barrier for hydrate nucleation is so high that hydrate formation occurs at higher relative humidities than the theoretically determined transition relative humidities [6]. Figure 13 shows an example of a DVS curve showing hysteresis.

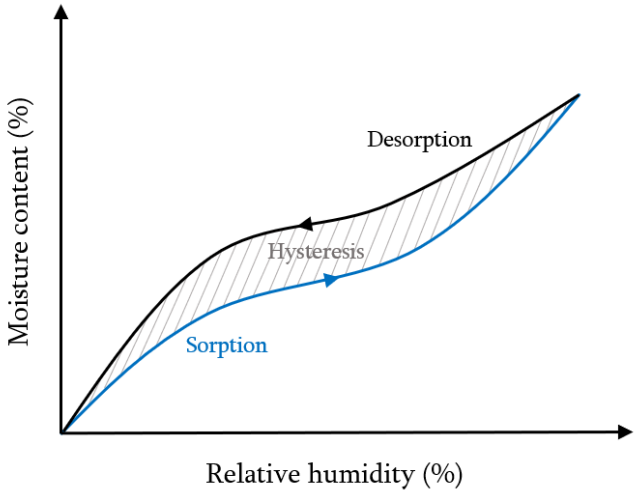

Figure 13. Theoretical DVS curve with hysteresis

2.3.2 Near-infrared spectroscopy

NIR refers to the region of the infra-red spectrum closest to the visible light region which is specified as the region lying between 400 cm^{-1} and 12000 cm^{-1}. This region is not associated with any fundamental transitions which are observed in the IR region, but rather with overtones and combination modes of molecular vibrations occurring in the infra-red. The bands in the resultant spectra are typically broad and can overlap making band assignment difficult. The spectra will change in time and visualize how the process behaves.

Compared to various Process Analytical Tools, NIR is one of the better methods used to analyse the water content in a substance with high accuracy. Water has strong sorption bands around 5128 cm^{-1}

and 6896 cm^{-1} that can be used for water determination with high sensitivity. These sorption bands correlate respectively to the combination of the O-H stretching vibration and the O-H bending vibration and the first overtone of the O-H stretching vibration [37], [38]. Samples can be analysed rapidly and in a non-invasive way using NIR [11], [15], [20]. Another advantage of NIR is that the PAT generates online data during the drying process. In this way, the drying process can be precisely monitored and stopped when the desired water content is reached [9], [12], [14], [16]. The complexity of analysing solids with NIR is that, unlike liquids, they are anisotropic. Meaning that the properties are not the same in all directions. In the study by Burgbacher et al. 2008, an in-line NIR probe was used to measure the solvent content in different dryers, namely a spherical, paddle and a filter dryer [9]. In other studies, an in-line NIR probe was used for monitoring fluidised bed drying processes [39]–[41].

The water content cannot be determined immediately in a NIR spectrum, only the sorption bands are measured. The water content can be obtained by establishing a calibration model. This model is constructed by assigning several spectra to the correct water content, for example, determined using a Karl Fischer titrator. On this data, multivariate analysis can subsequently be carried out. Here the most significant changes in the spectra are analysed and linked to the component of which the concentration is desired. Several models exist to obtain this, such as principal component analysis (PCA) and partial least squares (PLS) [11], [15]. These models have two objectives in the calibration. First, both models apply linear transformations to derive a set of independent variables from a set of highly correlated variables. The second purpose of both models is to reduce variables [42]. The difference between PCA and PLS is the fact that PLS is a supervised method that gets its information from known input data of the samples and thus also links these values to the variations apparent among the various spectra. PCA, on the other hand, is an unsupervised method and therefore does not include data from the samples. the output of a PCA model is a certain number of principal components (in application with NIR these are wavelengths at which variation between the spectra is visible) that explain the observed variation in the output data. Thus, if data from the samples are known, the PLS model is usually preferred.

2.3.3 Thermogravimetric analysis

The thermal stability of a component can be analysed with thermogravimetric analysis (TGA). This technique measures the quantity of volatile substance present by measuring the weight difference occurring when a sample is heated to a specific temperature. The temperature and heating rate can be programmed in a run-through programme. Typically, this method is conducted in an inert environment using a nitrogen flow [43]. In the study by Ronkart et al. 2010, TGA is used to analyse the thermal properties of a monohydrate (1 mole water : 1 mole compound) and a hemihydrate (1 mole water : 2 mole compound) [44].

TGA is an important technique in the characterisation of hydrates and solvates. With this technique it is possible, for instance, to differentiate between bound and free water, with free water correlating to the first weight loss. The desorption of water is related to the type of water-solid interactions. A distinction can be made between water bound to the surface, capillary condensation, desorption out of disordered regions and bound hydrate water. These different natures of water each have a unique rate of desorption [6].

Often, TGA is combined with mass spectroscopy. This application is particularly interesting when several volatile substances are present, such as multiple solvents. TGA can only detect the weight loss and cannot distinguish between the different components. By adding MS to the outlet stream of the TGA, it is possible to identify these substances [22], [36], [45].

Chapter 3. Materials & Methods

A detailed description of the materials and methods used in this study is given in the paragraphs below. The APIs and other materials used are described in section 3.1. The realization of the humidified nitrogen flow was accomplished using a humidifier, described in section 3.2. Subsequently, in sections 3.3 and 3.4, the drying set-ups are described, divided into static and dynamic drying. The conditions of the drying experiments are shown in a summary table (Table 15) in the appendix. These conditions are briefly restated in the results and discussion for the applicable experiment. Next, sections 3.5 to 3.9 provides detail on the analytical methods used. Finally, the conditions used to determine the influence of ambient air on the water content of a sample are presented in section 3.10. The data analysis for compound B was performed using the software PI ProcessBook.

3.1 Active pharmaceutical ingredients

In this thesis, two different APIs were used. The first API is referred to as compound A and is a chlorohydrate salt. The exact type of this hydrate was unknown. This API was used for the experimental work performed in Beerse. The second API that was investigated is a typical channel hydrate and is referred to in this study as compound B. This API was already in production and the data collected in these batches were used in comparison with the findings obtained from lab experiments on compound A. The solvents used in this study are water, methanol and isopropyl alcohol.

3.2 Humidifier

To achieve a humidified condition during drying, the Cellkraft humidifier P-50 was used. The general function of the humidifier was to introduce water vapour into an otherwise dry nitrogen flow. By using a membrane humidifier, the nitrogen flow was humidified to the desired relative humidity. The working of the humidifier is shown in Figure 14 and Figure 15. It is important to note that the membrane was heated when higher humidity levels were required. As a result, the outgoing flow could differ in temperature compared to the operating conditions, which could result in a variation in relative humidity. The humidifier P-50 was capable of a nitrogen flow of 50 nl/min. This device was equipped with various sensors. The main process parameters used in this study are the relative humidity and temperature of the outlet flow and the temperature of the membrane. This unit distinguishes between low and high flow. In the case of low flows, the inlet flow was split, with one flow passing through the membrane and the other flow bypassed, as visible in Figure 15. The humidity was regulated by the ratio of both the 'wet' and dry flows. In the case of high flows, the entire flow was passed through the membrane, and the humidity was regulated by the temperature of the humidifier.

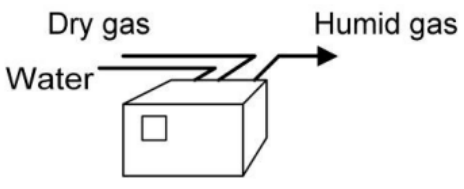

Figure 14. Schematic of humidifier

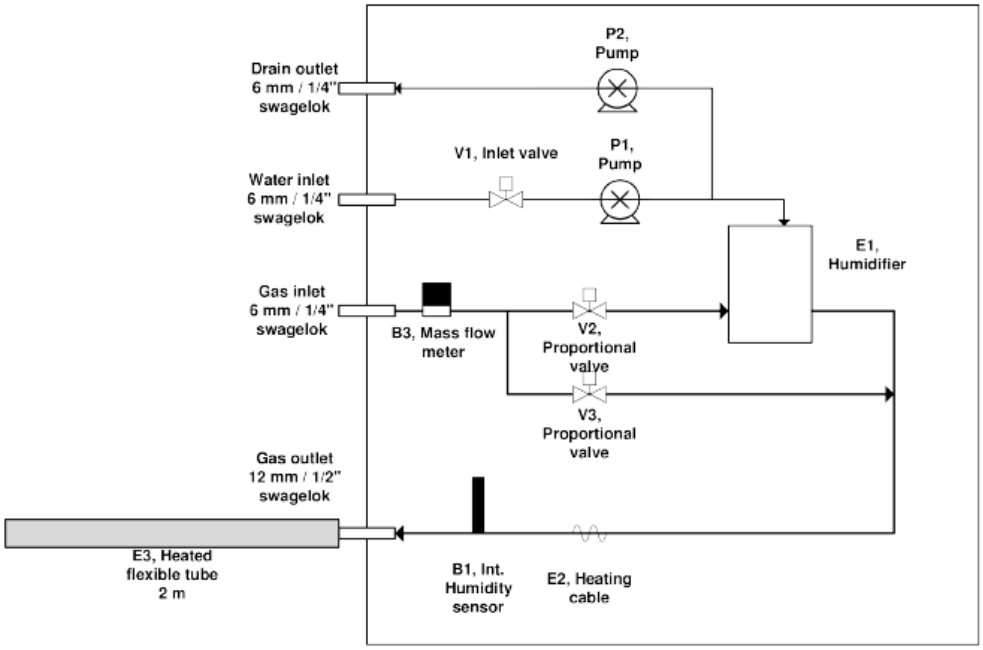

Figure 15. P&ID humidifier Cellkraft P-50

3.3 Static drying

3.3.1 Vacuum oven

A Memmert VO101 vacuum oven, equipped with an internal temperature and relative humidity sensor, was used to establish the static drying behaviour of compound A. This oven had been modified to allow a NIR or Raman probe to collect infrared/Raman spectra directly in the oven, as shown in Figure 16. Drying in the oven was accomplished using electrically heated surfaces combined with an applied reduced pressure (vacuum) and a small N_2 flow ('bleed') to efficiently remove headspace vapours. This flow ensured that the released water molecules could be removed from the oven and thus no condensation occurred. If the vapour pressure of the solvent dropped below the actual pressure (i.e. the vacuum), drying could not continue. The N_2 flow constantly refreshed the volume and thus prevented this problem from occurring. The desired relative humidity was obtained by passing an N_2 flow through a humidifier unit. In this way, the N_2 flow controlled the relative humidity in the oven. The drying process was analysed using NIR spectroscopy. This setup is shown in Figure 17. The parameters used during the drying experiments are shown in Table 15 in the appendix. For greater clarity in the results, these parameters are listed in short with the corresponding experiment in section 4.

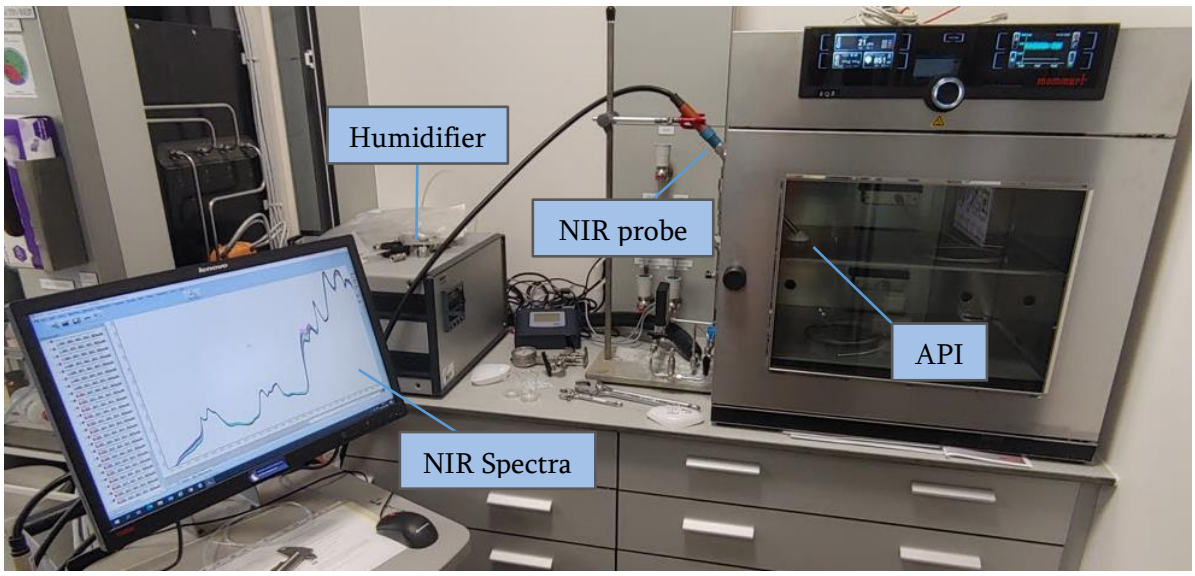

Figure 16. Setup vacuum oven, humidifier & PAT

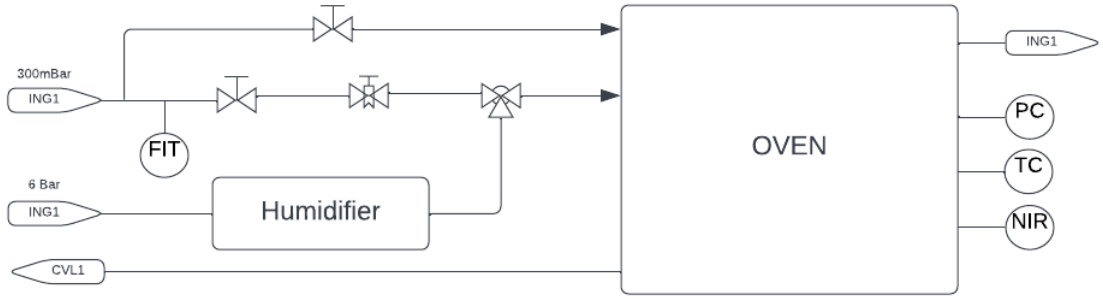

Figure 17. P&ID setup oven and humidifier

3.3.2 Filter dryer

In addition to the vacuum oven dryer, a custom built filter dryer was also used, as shown in Figure 18. This filter dryer was not capable of heating and was equipped with a window to allow measurements of NIR spectra through the window. In this filter dryer, the API was dried by passing a dry or humidified nitrogen flow through a cake of the API. In this way, the drying was static, but the contact surface between the nitrogen and the API was larger than the vacuum oven dryer. Therefore, the disadvantage of static drying was eliminated and considerably lower drying times could be achieved, which was ideal for smaller drying experiments. The conditions of the drying experiments are shown in Table 15 in the appendix.

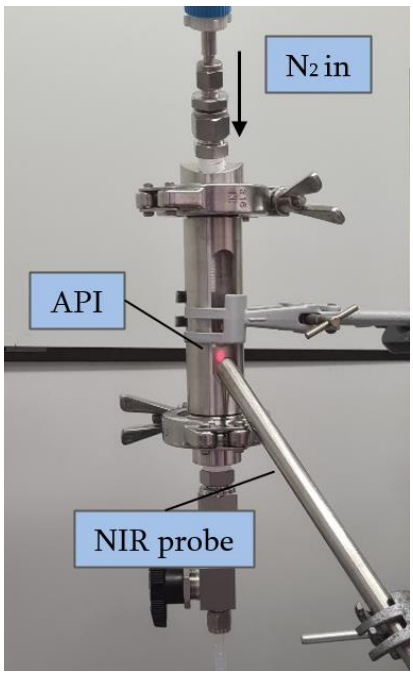

Figure 18. Setup filter dryer

3.4 Dynamic drying

For the dynamic drying experiments, the OptiMax 1001 Thermostat from Mettler Toledo was used. This dryer was equipped with a heated jacket and was connected to a vacuum pump, which allowed working under reduced pressure. Similar to the vacuum oven dryer, a nitrogen flow ('bleed') was used in this process. Again, a humidifier was used to obtain a humidified nitrogen flow. Temperature, pressure and NIR measurements were carried out in the powder during drying. The agitated dryer used in this study is shown in Figure 19 and the drying conditions are shown in Table 15.

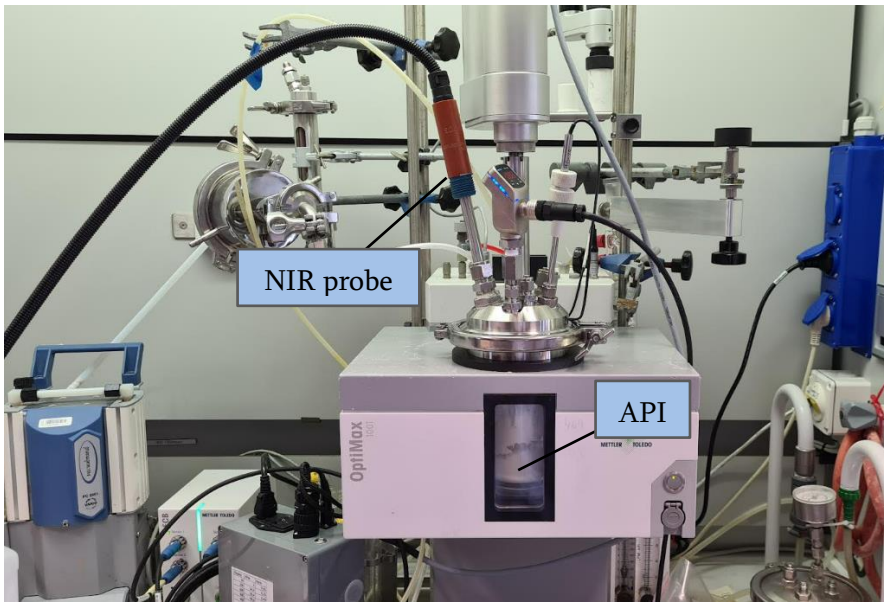

Figure 19. Setup agitated vacuum dryer

3.5 Dynamic Vapour Sorption

Vapour sorption analysis (VSA) was used to determine the water content in function of the water activity. The vapour sorption analysis was carried out with a Decagon Aqualab Vapour Sorption Analyser, using a dew point type sensor. In this analysis, the water content of the initial sample was included, measured with Karl Fisher. Using this DVS curve, the water content of a sample could be calculated from the current water activity of the ambient atmosphere and thus the sample, which could be measured using VSA as well. The vapour sorption analyser is shown in Figure 20.

In this study, the DVS was carried out twice for compound A. The first analysis was performed at a temperature of 25°C. The water activity was varied in steps of 0.1 and each step was held for 2 hours to reach equilibrium. The water activity was varied from 0.03 to 0.95 and one cycle of adsorption and desorption was performed. The second analysis went through the same program as the first, but at 40°C. Finally, both DVS curves were transformed into a combined DVS curve

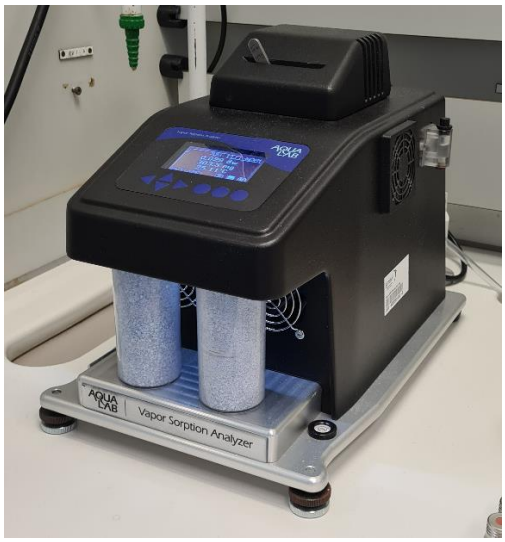

Figure 20. Decagon Aqualab Vapour Sorption Analyser

3.6 Near-infrared spectroscopy

The water content was analysed using a Matrix F near-infrared spectroscope from Bruker and with the help of a solid probe. In contrast to a liquid probe, the light in a solid probe was divided into several outputs. A solid is in fact anisotropic, meaning that its properties vary due to changes in orientation of the sample. To reduce this effect, multiple outputs of light were used instead of one, as is the case with liquid probes. An example of a solid probe is shown in Figure 21. In this study, NIR spectroscopy was used for both analysing samples offline and analysing the API during the drying process. In combination with a calibration, the water content could be determined online during the drying process. The spectra shown in the results were all treated with vector normalization as pre-processing.

Figure 21. Schematic of a solid probe [46, p. 1]

3.6.1 Calibration

For the calibration of the NIR for the determination of the water content, the OPUS software was used. This software had a built-in function for creating a model using known water contents. These water contents were determined by means of Karl Fisher titration. Next, this data was linked to the correct NIR spectra, and a model was created, using partial least squares (PLS) regression. Further information on how the model was obtained and optimised is given in section 4.1.

3.7 Thermogravimetric analysis

Thermogravimetric analysis was performed using a TGA/DSC 3+ device from Mettler Toledo, shown in Figure 22. In this study, two pre-programmed heating procedures were used. A first procedure consisted of heating to 50°C, after which this temperature was maintained for 60 min. Subsequently, in a period of 30 minutes, the temperature was rapidly increased to 180°C. A second procedure used a more rapid method to obtain a quick overview of the amount of solvent present on the API. This procedure consisted of heating to 180°C in 6 minutes.

Figure 22. Mettler Toledo TGA/DSC 3+

3.8 Gas chromatography

The analysis of the solvent content present in the API (MeOH and IPA) was carried out using headspace gas chromatography (GCHS). This was conducted offline on samples collected before, during and after the drying process. The preparation procedure consisted of the following: a specific mass of the API, depending on the expected amount of solvent, was weighed and dissolved in 2 ml of 1,3-Dimethyl-2-imidazolidinone (DMI). These measurements were performed by the Process Analytical Research (PAR) department within Janssen Pharmaceutica.

3.9 Karl fisher titration

For the analysis of the water content used to establish the calibration model for the in-line near-infrared spectroscopy application, coulometric Karl Fisher titration was used. Like the GCHS, this analysis was performed on offline samples of compound A with varying water content up to approximately 10%. Karl Fisher titration is based on an oxidation reaction between iodine and sulphur dioxide. The analysis is complete when all the water present in the sample to be analysed has been consumed. The water content is determined by the amount of iodine that has been used. In the coulometric method, this iodine is generated electrolytically and in the volumetric method, a solution containing a known quantity of iodine is added to the sample [47], [48]. Also these measurements were performed by the Process Analytical Research (PAR) department within Janssen Pharmaceutica.

3.10 Influence ambient air on the water content

To determine the effect of the ambient air in the headspace of a vial on the water content, the following experiments were carried out. In the first experiment a sample with an initial water content of 1.0% and a MeOH content of 5.5% was used. Different vials were filled, each with a different headspace. The ratios between the headspace and the API are shown in Table 2 and Figure 23. A completely filled vial (no headspace) was used as a blank sample for the anisotropic effect of the powder during the NIR analysis. Three vials of each ratio (API/HS) were prepared. One of these three vials was opened 5 times for about 30 sec. The other two vials were closed from the beginning such that only the headspace had an effect on the sample. The results of these two vials were combined. The relative humidity at the beginning of the experiment was 27.4% (and thus also the RH inside the closed vials at the start) and during the experiment, the RH of the room varied between 30 and 40%.

Table 2. Ratio API/Headspace

Sample	Volume API (ml)	Volume headspace (ml)	Ratio (API/Headspace)
Blank	12.0	0.0	1/0
1	5.8	6.2	1/1
2	1.7	10.3	1/6
3	2.1	18.9	1/9

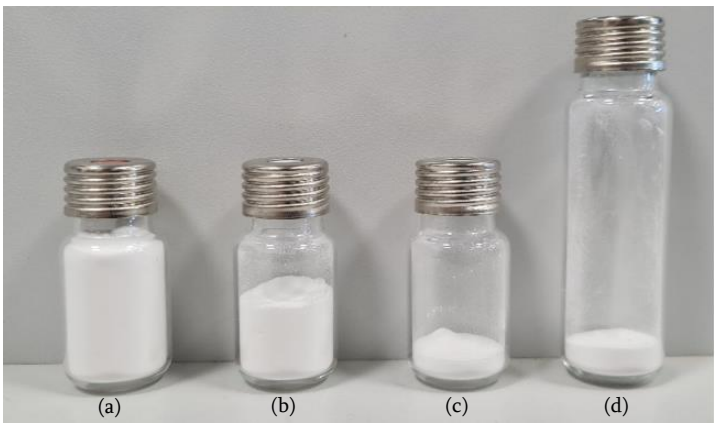

Figure 23. Ratio API/Headspace; (a) blank; (b) 1/1; (c) 1/6; (d) 1/9

The conditions of the second experiment were similar to those of the first experiment. Here a sample was used with an initial water content of 1%, MeOH content of less than 500 ppm (0.05%) and an IPA content of less than 500 ppm. The relative humidity at the beginning of the experiment was 29.7% and during the experiment, the RH varied between 30 and 40%. All these experiments were analysed for water content using near-infrared spectroscopy. Each measurement was repeated three times and the average value was calculated.

3.11 Process data compound B

The process data of compound B was monitored and processed using the software PI Processbook. Figure 24 shows the complete trend that was used in this thesis and represents the drying process of Compound B. This drying process was carried out intermittently, meaning that the agitator did not work during the entire drying process. In this way, drying was partly static and partly dynamic. Further on in this thesis, zoomed in figures of this trend are displayed in which the behaviour of these trends are described in more detail.

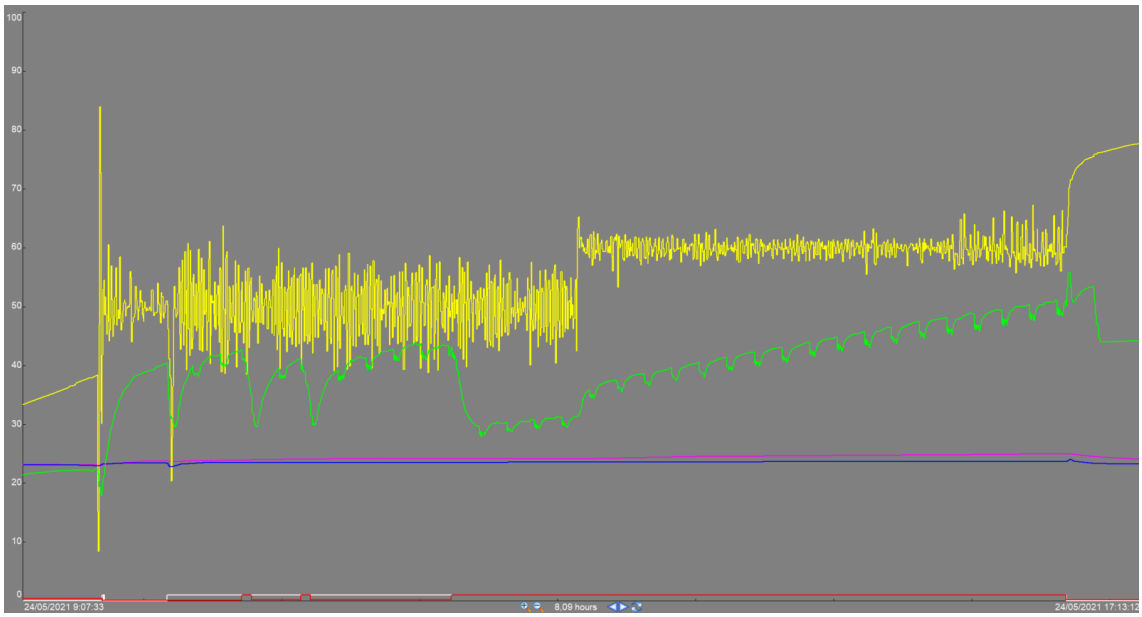

Figure 24. Complete trend drying compound B; (Yellow) RH inlet (%); (Green) RH outlet (%); (Pink) Temperature inlet (°C); (blue) Temperature outlet (°C); (Red) RPM agitator; (White) Vacuum pump (ON/OFF)

Chapter 4. Results & Discussion

In this chapter, the results of the different drying experiments are described, discussed and compared. In section 4.1, specifications of the model obtained for the in-line near-infrared spectroscopy are presented. The results achieved using the DVS analysis are discussed in section 4.2. These provide a useful insight into the amount of water compound A can adsorb at a specific relative humidity. Furthermore, the influence of ambient air, both directly and in the headspace of the vial, is demonstrated. The following sections contain the results of multiple drying experiments with different drying conditions. The influences of these conditions are illustrated by means of different analytical methods. In addition to the results of the drying experiments, the process data of the drying process of compound B is used to confirm and strengthen the conclusions. These data originate from a large scale production and give therefore an idea of the impact of this scale-up. Finally, in section 4.8, the humidifier is characterised using the vacuum oven setup.

4.1 NIR calibration

Monitoring the water content during the drying process using NIR spectroscopy allowed to track the sorption of water to or from the product and proved very useful as an in-line process analytical technology. In addition, it was possible to determine water content from the intensity of several bands (5128 cm^{-1} and 6896 cm^{-1}) in the spectra using a regression model. In order to obtain a model, several spectra had to be correlated with samples with a known water content. These water contents were determined by Karl Fisher titration. An important factor for a good model was that a sufficiently wide range of data points was defined. The software subsequently presented a number of pre-processing and optimisation options, based on the specified spectra and the variation between these spectra. The model was improved throughout the study by adding more data points.

During the first stage of the thesis, MeOH was used as a final washing step before the drying process. Consequently, the model was composed using data from samples containing API, water and MeOH. Afterwards, another solvent was introduced as a final washing step, namely IPA. However, when analysing these samples using the NIR model at that time, incorrect values were noticed. The reason was the introduction of IPA into the system. Due to the use of a new component, the NIR spectra contained new peaks and thus new changes to which the model had not been adjusted. For this research, it was important to include data points from both the MeOH wash and the IPA wash in the model.

As a pre-processing procedure, the first derivative and vector normalization (SNV) were applied to the data. The model consists of 27 data points, each of which was correlated with three measured spectra. The reason for this was to account for the anisotropic effect of the powder. Figure 25 shows the predicted water content value compared to the experimentally determined water content value. Figure 26 shows the deviation between the predicted value and the effective value.

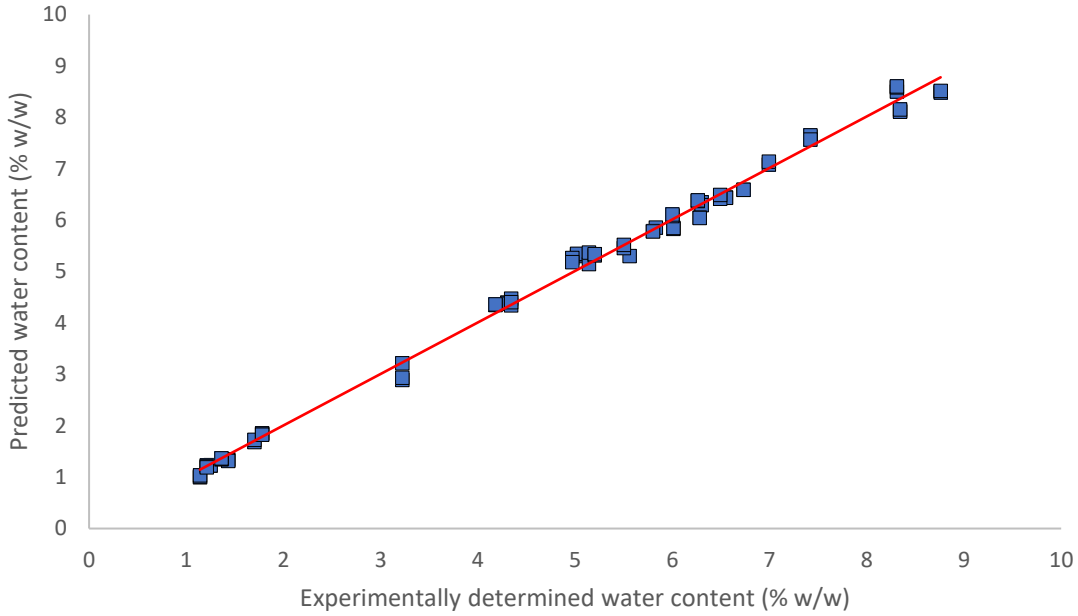

Figure 25. Prediction vs experimentally determined water content

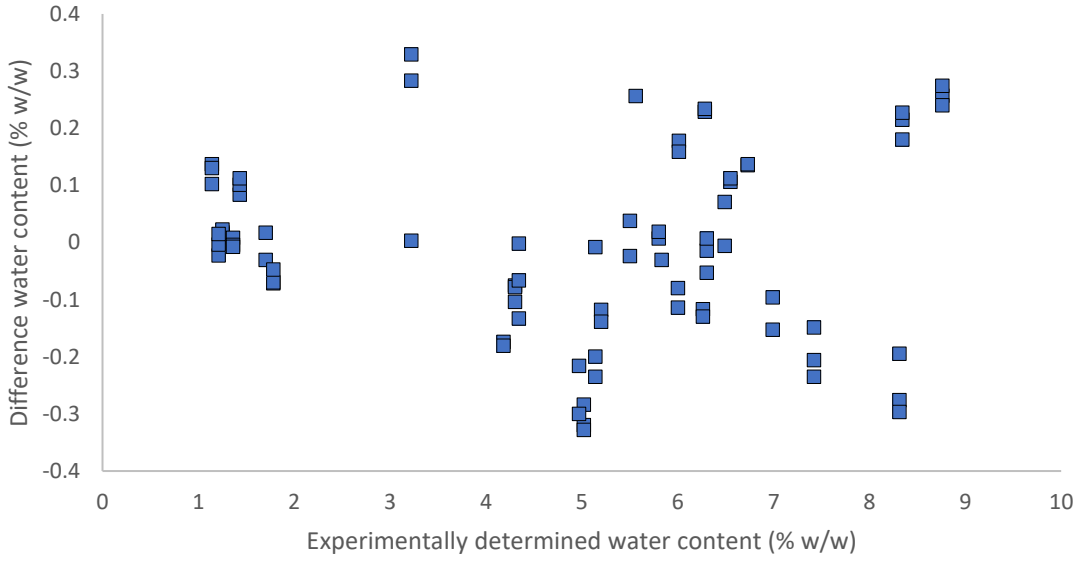

Figure 26. Difference vs experimentally determined water content

The wavenumber regions considered for this model were from 7500 to 6100 cm^{-1} and from 5452 to 4600 cm^{-1}, as shown in Figure 27. According to the model, these regions showed the highest variation between the data points. These regions were in line with the water peaks of 5128 cm^{-1} and 6896 cm^{-1} found in literature, which correlated respectively to the combination of the O-H stretching vibration and the O-H bending vibration and the first overtone of the O-H stretching vibration [37], [38]. The R^2 value of the model equalled 99.4% and, as shown in Figure 26, the largest deviation between the true value and the predicted value was 0.33% w/w. During further investigation it was noted that this deviation was mainly due to the anisotropic effect of a powder. If a drying process was followed up statically with the probe positioned at the same point on the

API, this deviation was considerably lower. The range of the model was from 0.72 to 8.76% w/w since this was the range of water content most relevant for compound A. The first derivative pre-processing of the spectra in Figure 27, is shown in Figure 28.

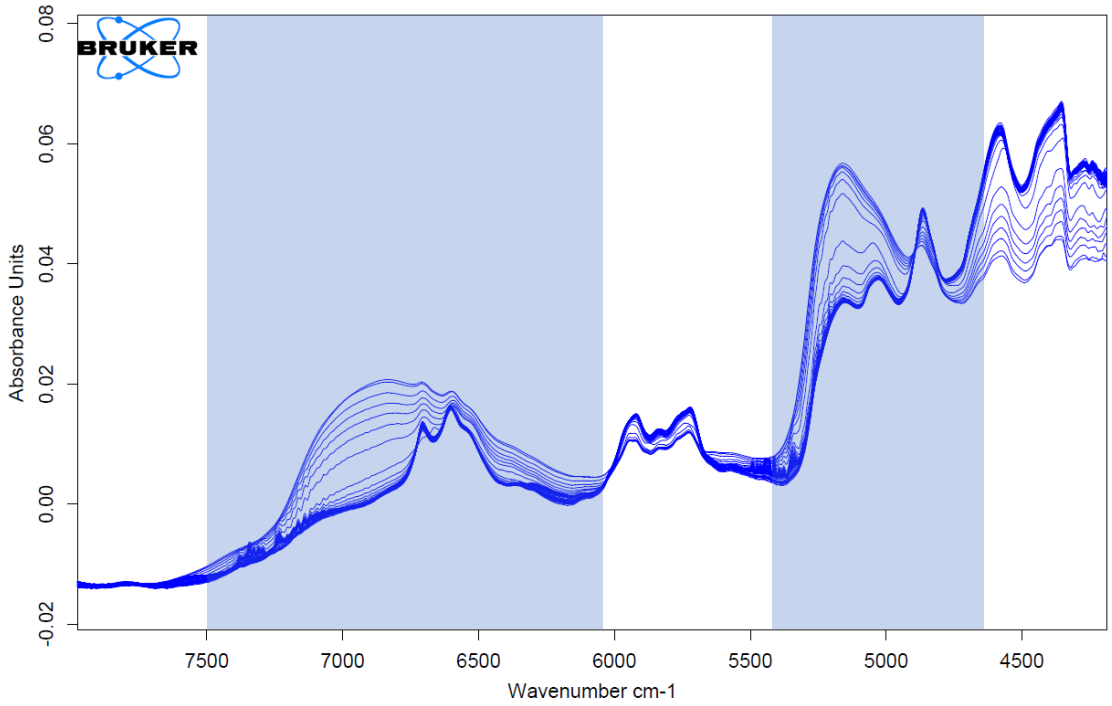

Figure 27. NIR spectra with regions 7500 - 6100 cm $^{-1}$ and 5452 - 4600 cm $^{-1}$

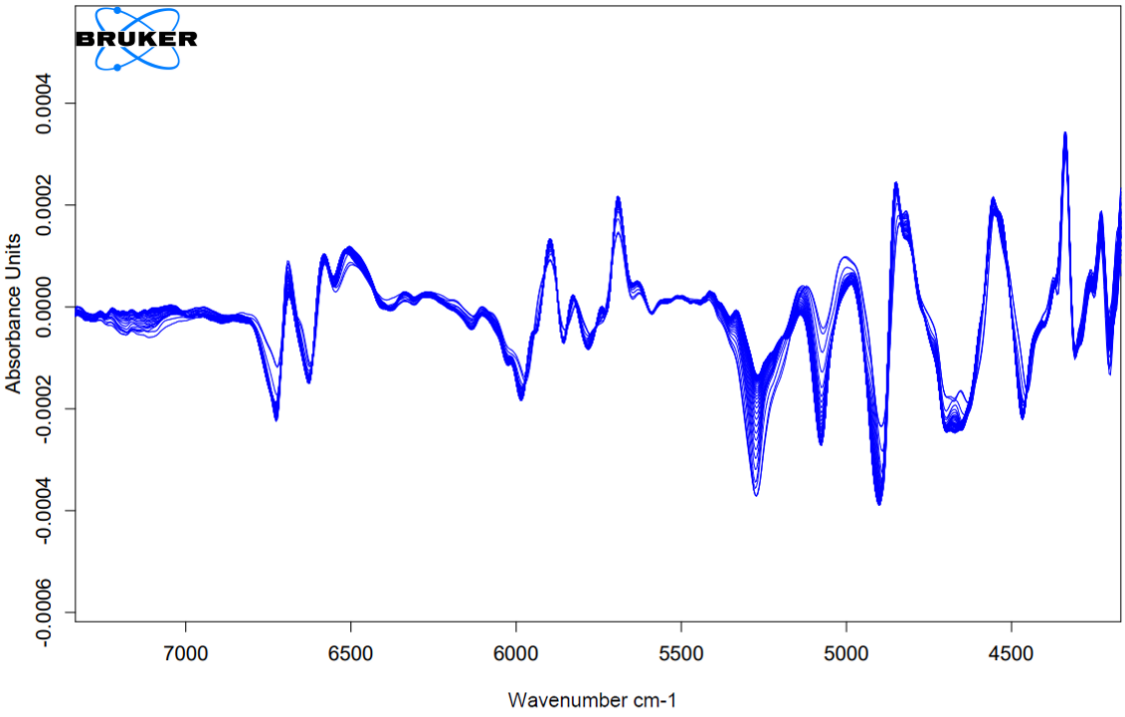

Figure 28. NIR spectra after first derivative pre-processing

In Figure 27, variations in the spectra were apparent in the region of 4500 cm^{-1}. Since no MeOH uptake or release occurred in this sample, these could not be linked to MeOH. In Figure 28, where the same spectra are displayed after the first derivative pre-processing procedure, these variations were no longer visible. This demonstrated the working and importance of the pre-processing method. The variations of the water peak in the region between 5000 and 5500 cm^{-1} were still visible in Figure 28.

In addition to constructing a model for the water content, the option of establishing a model for IPA and MeOH was also considered. This model focused on the area around 4400 cm^{-1}, shown in Figure 29. This region correlated to the combination vibration of O-H stretching and C-O stretching. Additionally, the region from 4000 to 4400 cm^{-1} correlated to the combination vibration of C-H stretching and bending [49]. However, these models were not accurate enough at or below the specification limit for both solvents (for MeOH<3000 ppm, for IPA<5000 ppm). Therefore, the NIR spectra were only used for a visual indication of the decrease in solvent content.

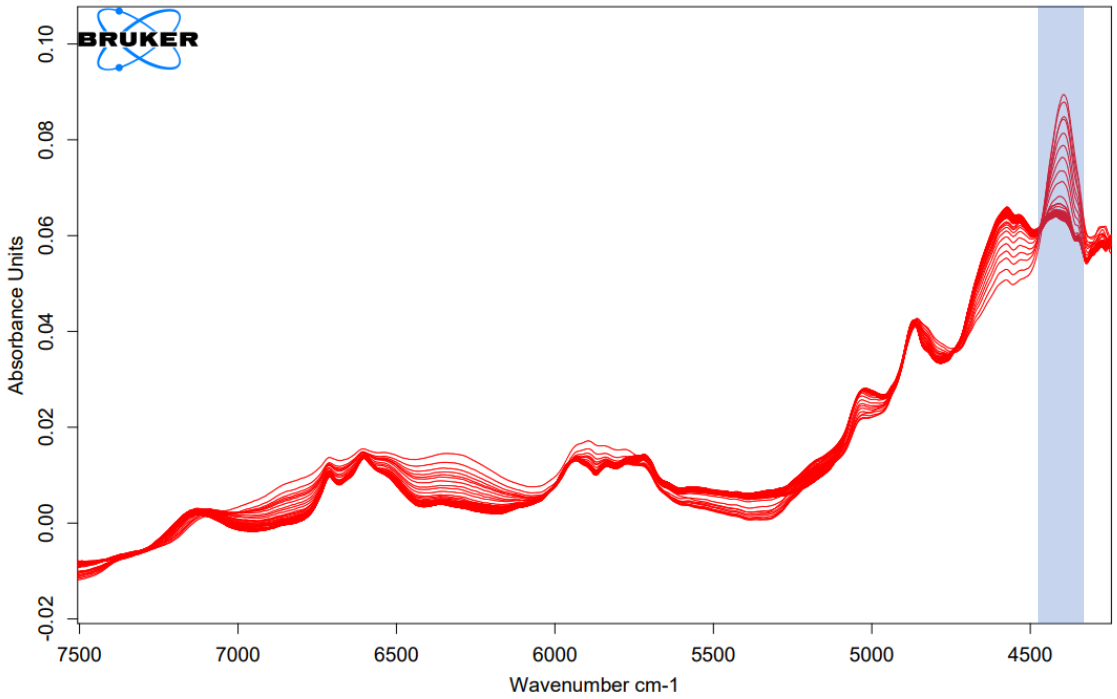

Figure 29. NIR spectra with region 4400 cm $^{-1}$

4.2 Dynamic Vapour Sorption

Prior to a drying process, it was important to obtain a clear understanding of the sorption behaviour of compound A. For this purpose, a DVS was performed. The initial water content of the sample was 3.58% w/w and was specified at the start of the analysis. This value was obtained in advance using Karl Fisher titration. As a result, the water content on the y-axis was the true value. The DVS curve of compound A is shown in Figure 30.

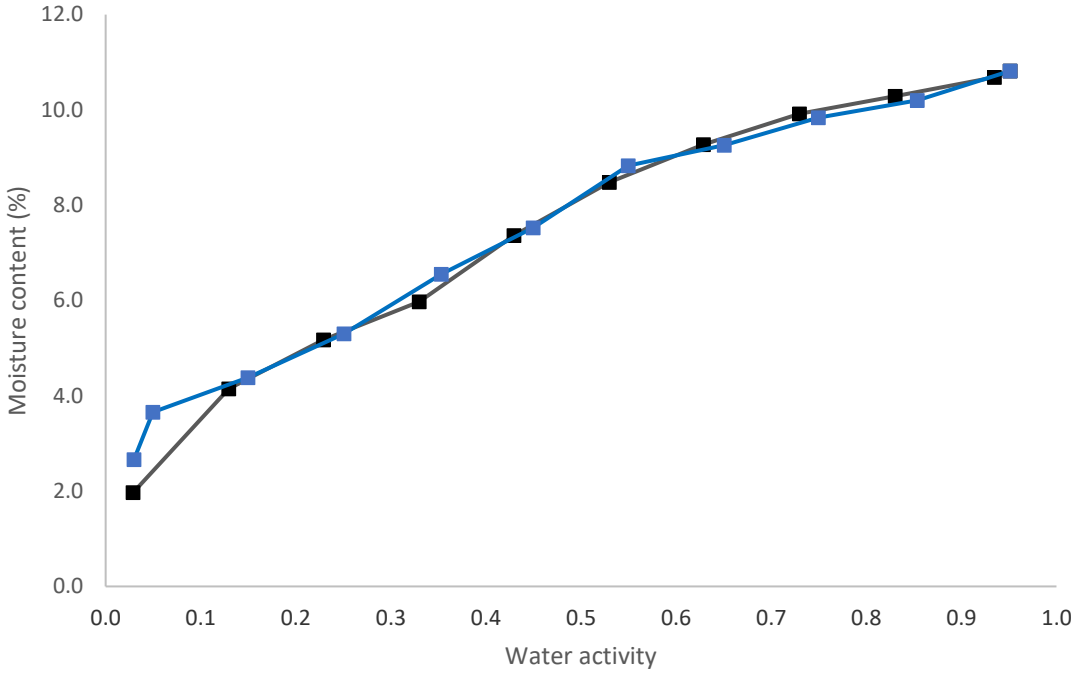

Figure 30. DVS compound A; (black) adsorption; (blue) desorption

From Figure 30 it can be concluded that compound A could adsorb and retain a maximum of 11% w/w of hydrate water. Also noticeable was that no hysteresis was visible in the region above a water activity of approx. 0.13. In this region, water was as easily adsorbed as desorbed. At a water activity lower than 0.13, a small hysteresis seemed to be visible. Whether this was in fact a hysteresis, was uncertain as the adsorption curve (black) in this region was based on only two data points. In contrast, the desorption curve (blue) in this region was based on three data points. However, the steeper section of the desorption curve (blue) indicated that at low water contents, it became more difficult for the water molecules to leave the crystal structure. If the compound exchanged hydrate water to the environment, the least strongly bound water was removed first, as this was the most easily released. Consequently, the last hydrate water experienced the strongest interaction with the crystal structure and was thereby more strongly bound. As a result, a higher driving force was required for the removal of the water molecules at low water activity. Furthermore, this DVS curve was used to determine the relative humidity required to reach a specific water content.

4.3 Influence of ambient air on water content

4.3.1 Ambient air in the lab

Before discussing the influence of the ambient air on the water content of the sample, the water activity of the surrounding air in the lab had to be visualized. This provided information on the number of water molecules available to exchange. Figure 31 shows the relative humidity and temperature measured in the lab during a period of one month.

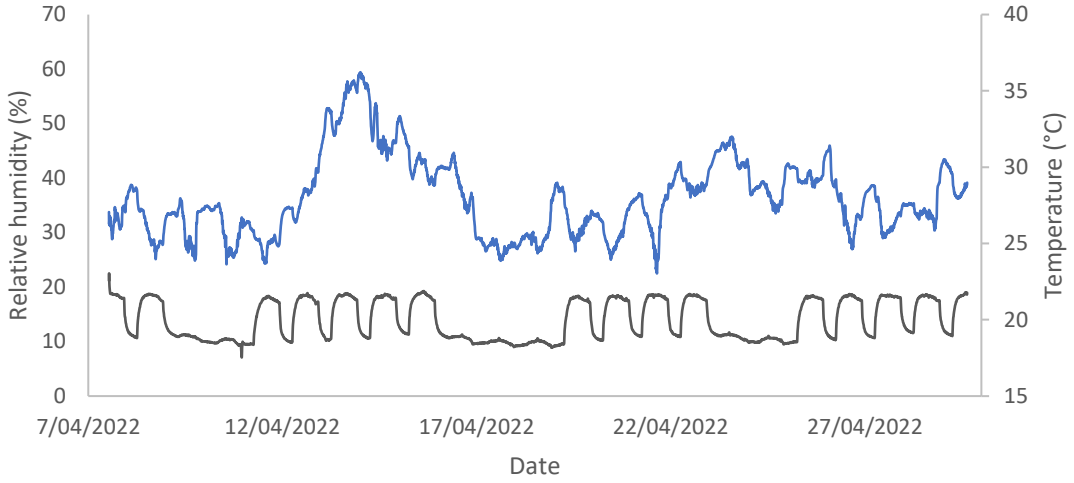

Figure 31. Relative humidity (blue) and temperature (black) monitored in the lab

As visible in Figure 31, the relative humidity varied considerably. The average value measured was 36.4% with a minimum value of 22.5% and a maximum value of 59.4%. At the beginning of this research values below 20% and even 12% were measured, but these are not shown in Figure 31. The relative humidity in the lab depended mainly on the weather and the treatment of the air in the building (e.g., heating of incoming air in winter). For example, on rainy days the air contained more water, so the relative humidity measured in the lab was also higher. Thus, it was important to consider the relative humidity present in the lab, as it was one of the driving forces of water exchange. The temperature trend in Figure 31 shows a clear repeated pattern. These increases and decreases could be linked to the central heating of the building. The temperature fluctuated roughly between 17 and 23°C, 23°C during the day when the heating was on and at night and during the weekend the temperature dropped to approximately 17°C. Also this was important to consider as the temperature in the lab could affect the temperature at the outlet of the humidifier. This could consequently increase or decrease the temperature difference between the oven and the outlet of the humidifier. This phenomenon is further discussed in section 4.8.

In several drying experiments, in which the water content was monitored using in-line NIR spectroscopy and subsequently analysed using Karl Fisher titration (KF), the results of both analytical methods did not match. At first, it was assumed to be a result of an incorrect calibration of the NIR. However, it turned out to be due to the influence of the ambient air between both analyses. By opening samples 3 to 4 times for other analyses, the API was exposed to the ambient air on several occasions and the air in the headspace of the sample vial was refreshed so that the sample could re-equilibrate with the headspace on every occasion. Table 3 shows the water contents determined using NIR and KF for three specific experiments.

Table 3. Water content determined with NIR vs Karl Fisher titration

Test	NIR before KF (% w/w)	NIR after KF (% w/w)	Karl Fisher coulometric 120°C (% w/w)
1	9.1	8.3	8.3
2	6.6	6.0	6.0
3	3.9	4.4	4.5
4	1.5	1.8	1.7

As shown in Table 3, the values of water content determined with NIR before KF and determined with KF did not match. The water content, determined with NIR before KF, referred to the NIR spectra at the end of the drying process. After performing the Karl Fisher titration, new NIR spectra of these samples were measured, whereby the values did correspond to those determined by KF. For the first two samples, the water content decreased between both analysis methods. The water activity of these samples, according to Figure 30, was approx. 0.6 and 0.4 respectively. Since the relative humidity at that time was lower than 40%, water was exchanged from a high (sample) to low water activity (ambient air) by desorption. The last two samples, on the other hand, adsorbed water between the drying process and the Karl Fisher analysis. Because these samples contained 3.9% and 1.5% water, according to the DVS curve (Figure 30), these samples would adsorb water in an environment with a relative humidity of 12% and higher (which was common in the lab as shown above). The extent of the difference in water exchange was dependent on various factors, such as the relative humidity in the lab, the size of the headspace in relation to the API, the behaviour of the compound regarding water and the time the vial was opened. So when the water content needs to be analysed, it is important that this is done before other analyses to minimize contact with the ambient air and to achieve a correct representative result.

4.3.2 Ambient air in the headspace

The influence of ambient air in the headspace of a sample was further studied. The sample used in the first experiment initially contained a water content of 1% and a MeOH content of 5.5%. Four different ratios of API/HS were used, of which the vial without headspace was used as a blank. For each ratio, there was a vial that was closed for the complete duration and a vial that was opened 5 times. RH at the beginning of the experiment was 27.5% and during the experiment, the RH varied up to 40%. The samples were analysed by NIR spectroscopy and the water content was determined with the previously established model. The results of the samples at the beginning, after 10 hours and after 38 hours are shown in Figure 32.

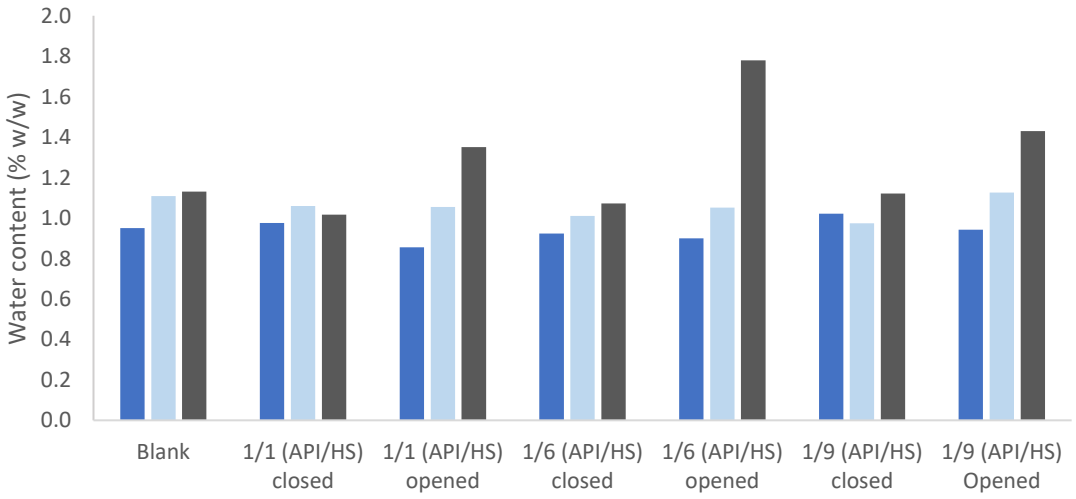

Figure 32. Water content in different ratio (API/Headspace) in methanol solvate; (blue) after 0 days; (light blue) after 10 days; (grey) after 38 days

As can be seen in Figure 32, hardly any water was exchanged in the closed samples. These samples were not opened during the experiment, meaning that only the headspace could influence the water content. The difference in water content in these samples was not greater than the difference in the

blank sample. However, a difference was visible in the samples that were opened five times during the complete experiment for approximately 30 seconds. The water content measured after 38 days (shown in grey) increased, indicating adsorption of water. By opening the samples, the headspace was replaced, which made more water available for exchange. However, the water adsorption was not great, as the highest increase was approximately 0.8% after 38 days. An explanation could be the presence of methanol (5.5%), which caused the water adsorption rate to drop. Since the sample was a methanol solvate, water had to displace the MeOH molecules in the crystal structure. This phenomenon was more difficult than a normal adsorption of water. To confirm this conclusion, the following experiment was performed, using a sample with an initial water content of 1% and less than 0.05% MeOH present. The result of this experiment is shown in Figure 33.

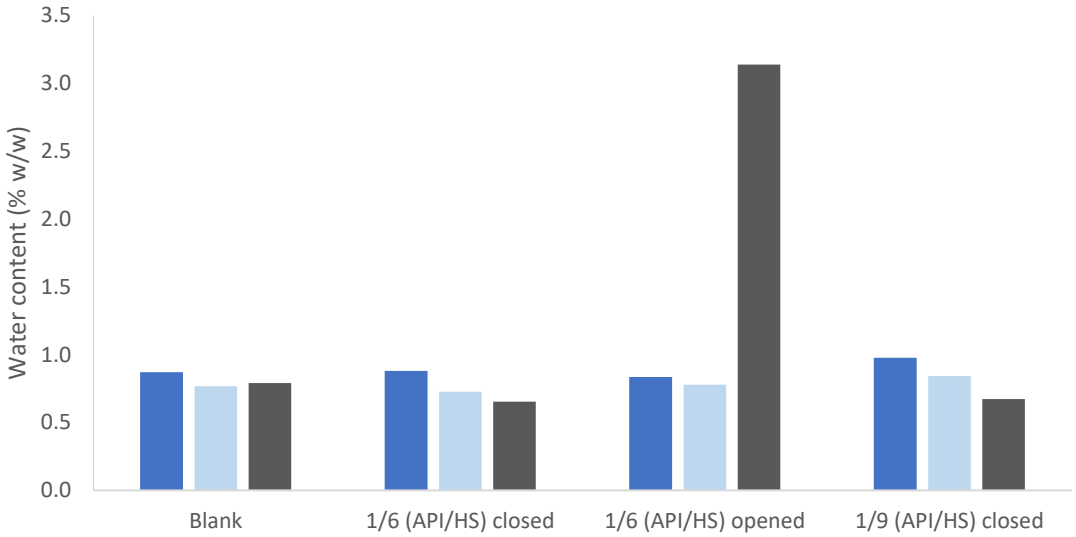

Figure 33. Water content in different ratio (API/Headspace) in hydrate; (blue) after 0 days; (light blue) after 2 days; (grey) after 20 days

Figure 33 again shows no change for the samples that remained closed, indicating that the headspace alone had no major impact on the sample. For the sample that was opened five times for about 30 seconds, a clear increase was visible. After 20 days, an increase of approximately 2.3% could be seen, which confirmed the previously drawn conclusion. The samples of the first two experiments were opened at the same times and consequently affected by the same ambient air (RH). The sample without methanol adsorbed more water in less time compared to the sample with a methanol content of 5.5%. Figure 34 shows the water adsorption rate for a sample without MeOH opened continuously (infinite headspace) with a relative humidity of 48.6%.

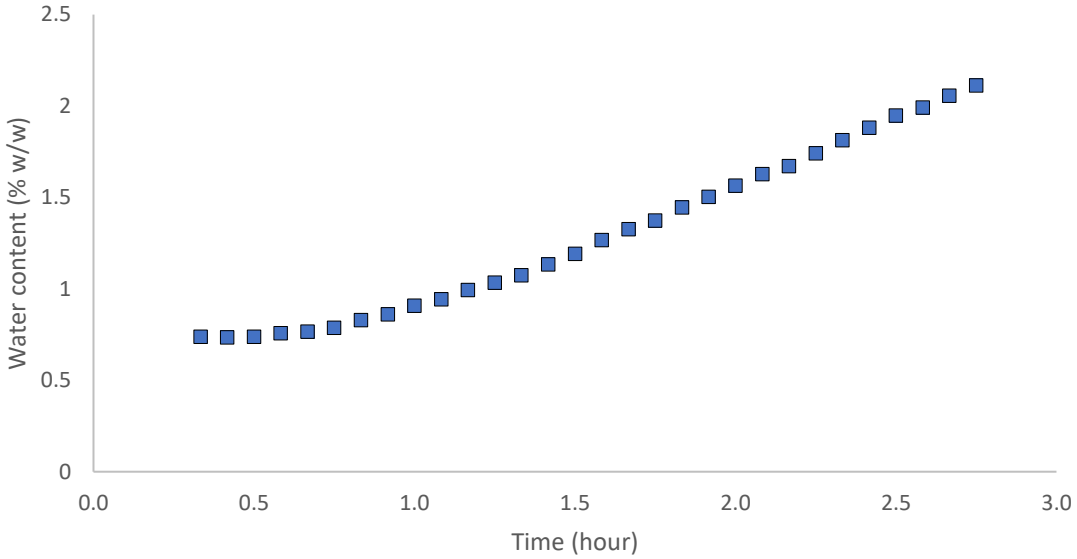

Figure 34. Water content opened vial with 0.05% MeOH at 48.6% RH

Figure 34 shows that a period of 1.5 hours resulted in a 1% increase in water content. From Figure 33 it was clear that the sample, which was opened five times, had an increase in water content of 2.3%. This sample was opened five times for approximately 30 seconds resulting in a total of approximately 2.5 minutes in direct contact with the ambient air. The increase in water content of 2.3% was therefore the result of the combination of direct contact with the ambient air and the renewal of the ambient air in the headspace. If a sample was immediately closed with a certain headspace, this headspace had only a limited influence. The combination of opening and thus refreshing the air in the headspace had a great impact on the water content of the compound. The impact of this combination is shown in Figure 35. In this experiment, a closed vial was analysed after opening this vial for a period of one minute at 27.4% RH. The API/Headspace ratio was 1/9. This result clearly showed an increase in water content, which confirmed the conclusion above.

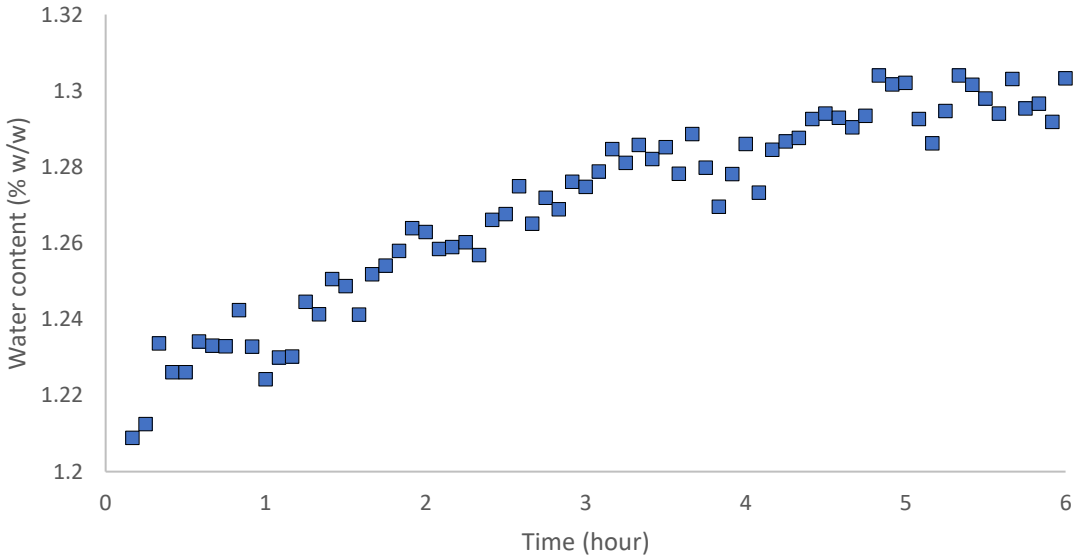

Figure 35. Water content closed vial with 0.05% MeOH at 27.4% RH

A final experiment was conducted to determine the effect of the headspace after closing a vial that had been exposed to the ambient air for several hours. For this experiment, a sample with an initial MeOH content of 5.5% and 1% water was used. First, the sample was exposed to the ambient air at a relative humidity of 38%. Subsequently, the vial was closed and the influence of the headspace on the water content was further analysed using NIR spectroscopy. The sample was analysed at the top and the middle of the powder, as shown in Figure 36. The results are shown in Figure 37.

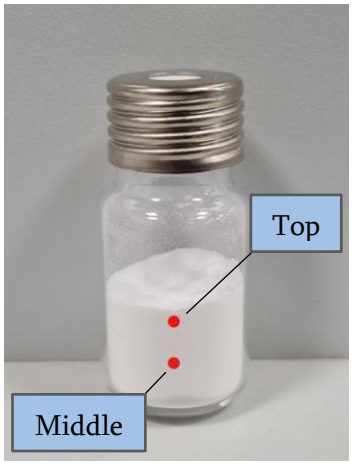

Figure 36. Positioning NIR probe measured at the top and middle

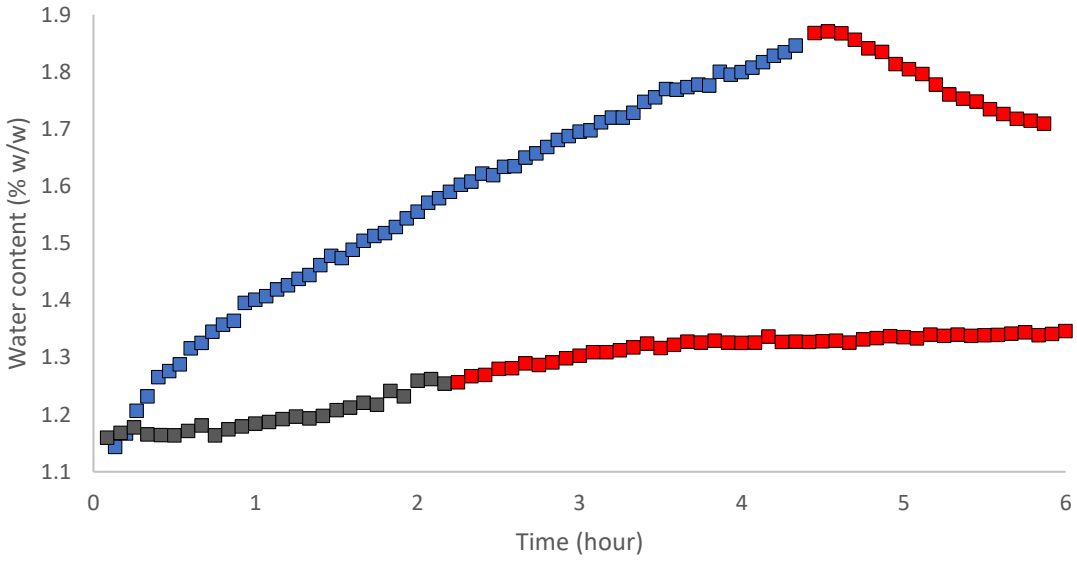

Figure 37. Water content opened vs closed vial with 5.5% MeOH at 38% RH

Several conclusions could be drawn from Figure 37. Firstly, a difference was visible between the water adsorption rate at the top of the powder (blue) compared to the rate at the middle of the powder (black). The reason for this was the fact that at the top, the water molecules were directly available from the ambient air. Deeper into the powder, fewer water molecules were present as they had to diffuse into the powder first. This phenomenon is further discussed in section 4.7. Besides the rate of adsorption, the behaviour after closing the vial (red) was of interest. At the top of the

powder, a decrease in water content was visible after closing the vial. The reason was that during the exposure of the sample to the ambient air, most of the water molecules were adsorbed to the top layer of the compound. When the vial was closed, these water molecules were distributed over the entire API until an equilibrium was reached. This observation was confirmed by the result of the water absorption measured in the middle of the vial. Here, after closing the vial, an increase was visible, which again indicated the distribution of the water molecules.

4.4 Static drying after MeOH wash

To gain an initial insight into the working of in-line NIR spectroscopy measurement, the drying behaviour of compound A and the humidifier oven setup, two static drying experiments were performed. The first drying process was divided into a drying step followed by a humidification step. During the second drying process, drying and humidification were performed simultaneously. Both experiments used a sample of compound A after crystallisation, washed with a MeOH-water mixture (35/65% v/v) followed by a second wash with MeOH. A Karl Fisher titration analysis and TGA were performed on this sample prior to the drying tests. The result of the TGA is shown in Figure 38.

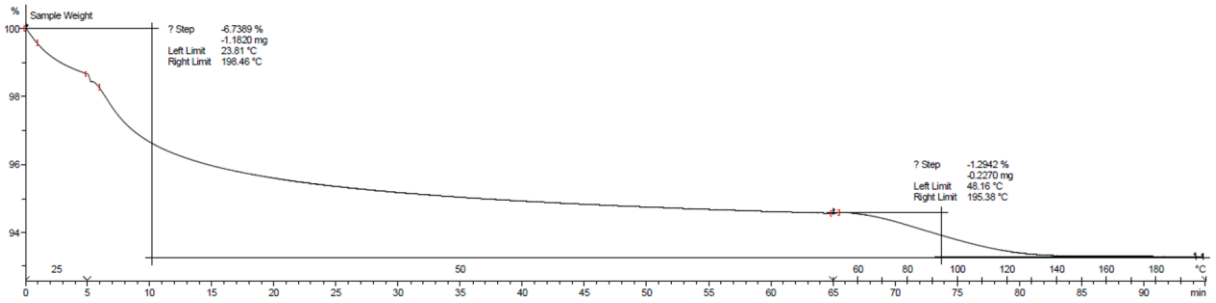

Figure 38. TGA before drying experiments

The Karl Fisher analysis showed a water content of 0.7%. On the TGA result in Figure 38, a total weight reduction of 6.7% was visible. Considering 0.7% corresponds to water, the remaining 6% was the MeOH content. The TGA showed just the total weight difference, which meant no distinction could be made between water and MeOH. In Figure 38, a plateau is apparent. For the first 60 minutes, a constant temperature of 50°C was maintained. Here a weight reduction of 5.4% was visible. After 10 minutes the slope started to decrease, which indicated a reduced release of solvent. More energy was required to remove the solvent, which suggested strongly bound solvent molecules. For the next 30 minutes, the temperature was strongly increased to 180°C, resulting in an additional weight decrease of 1.3%. Due to this high temperature, all bound solvent was removed. The parameters of the two experiments are shown in Table 4. The NIR spectra of the first dying experiment, the two-step drying process, are shown in Figure 39, Figure 40 and Figure 42. The spectra were collected every 1000 seconds.

Table 4. Parameters 2-step & simultaneous static drying experiment MeOH wash

	2-step drying		Simultaneous drying
	Drying	humidifying	
Flow (nlpm)	7	7	30
Temperature oven (°C)	40	21	21
Pressure oven (mbar)	200	200	950
Relative humidity (%)	0	87	48
mass sample (g)	3	3	3

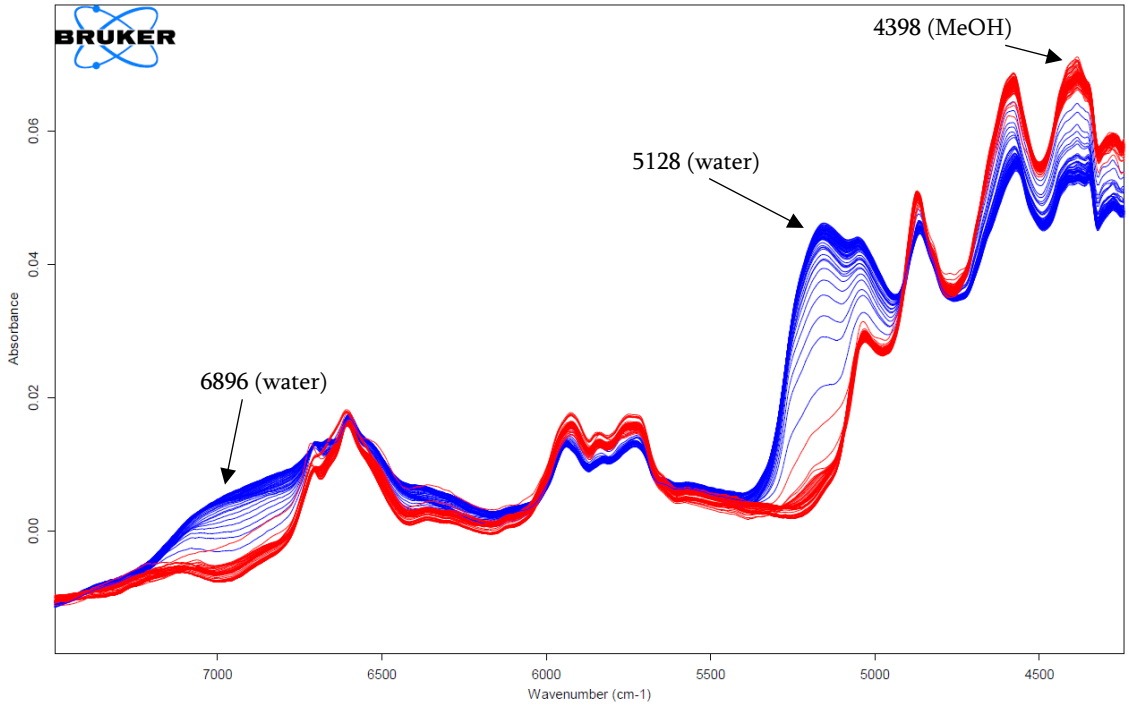

Figure 39. NIR spectra two-step static drying; (red) drying; (blue) humidifying

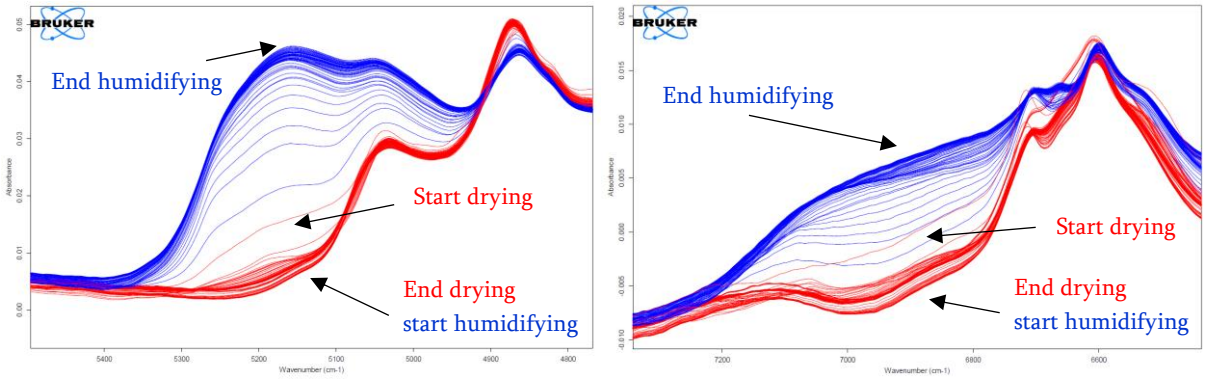

Figure 40. NIR spectra (detail) water sorption regions two-step static drying; (red) drying; (blue) humidifying

As shown in Figure 39, substantial variations were visible among the different spectra. The regions of focus in this study were the water peaks at 5128 cm^{-1} and 6879 cm^{-1}, shown in Figure 40. Here the water peaks decreased during the drying step (marked in red). Once switched to humidifying after 23 hours (marked in blue), a noticeable increase in these peaks could be observed. Using the

calibration model, these spectra were linked to a water content value. The results of this model are shown in Figure 41. In accordance with the spectra, a small decrease was visible during the drying step down to a water content of 0.5% followed by a strong increase of the water content up to 9.1% during the humidification step. According to the DVS curve, shown in Figure 30, a relative humidity of 87% would correspond to a water content of approximately 10%. It appeared that compound A had not reached equilibrium yet. Figure 41 shows a small increase still present at the end of the experiment.

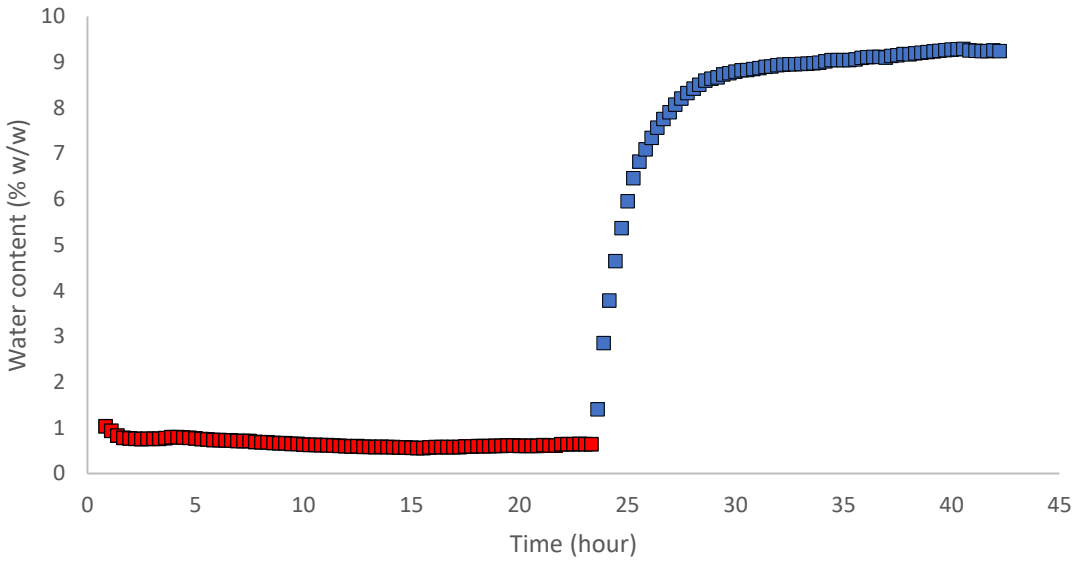

Figure 41. Water content two-step static drying; (red) drying; (blue) humidifying

Figure 42 shows the NIR spectra focused on the region around 4398 cm^{-1}, which corresponded to the MeOH content. During the drying step, a decrease in the MeOH content was visible in these spectra. However, it was noticeable that this peak continues to decrease once the humidifying step was initiated. This indicated that water was required to remove the low concentrations of MeOH from the API. At this point, MeOH was strongly bound to the crystal lattice and could not be removed under these drying conditions. By initiating water molecules, they displaced the MeOH molecules and consequently removed them out of the crystal structure. This phenomenon had also been described in other literature [22].

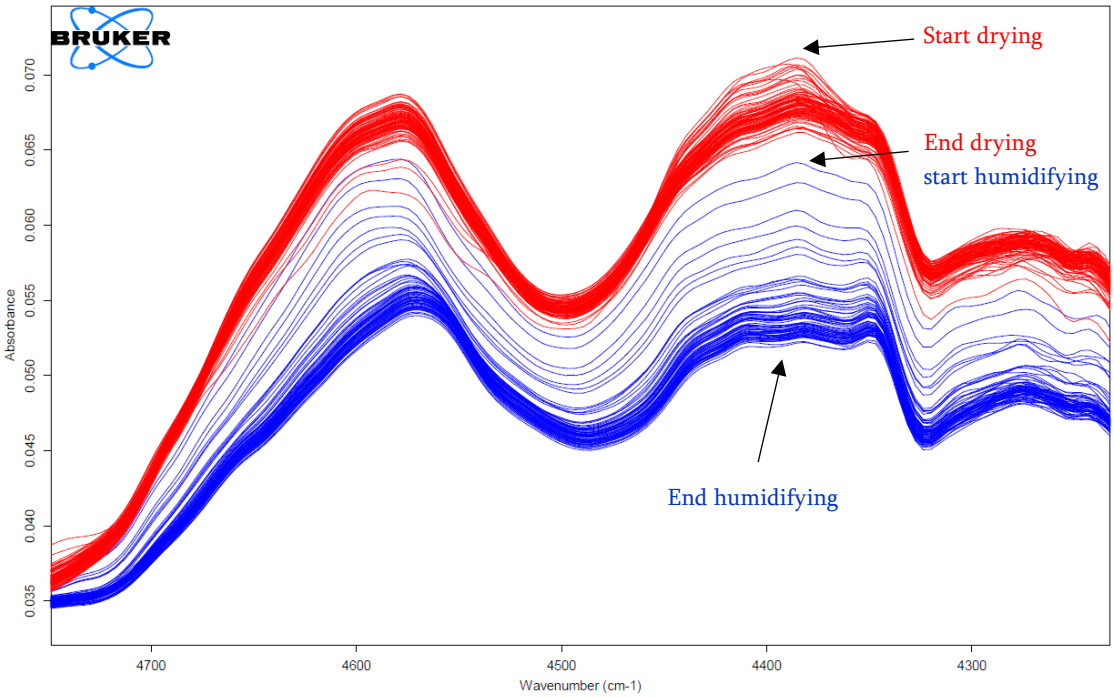

Figure 42. NIR spectra (detail) MeOH sorption region two-step static drying; (red) drying; (blue) humidifying

The NIR spectra of the simultaneous static drying experiment at 48% RH are shown in Figure 43, Figure 44 & Figure 45. Also in this experiment, the spectra were collected every 1000 seconds. Again, large differences in the spectra were apparent during drying. Since humidifying and drying were performed simultaneously, the water peak increased from the start of the process.

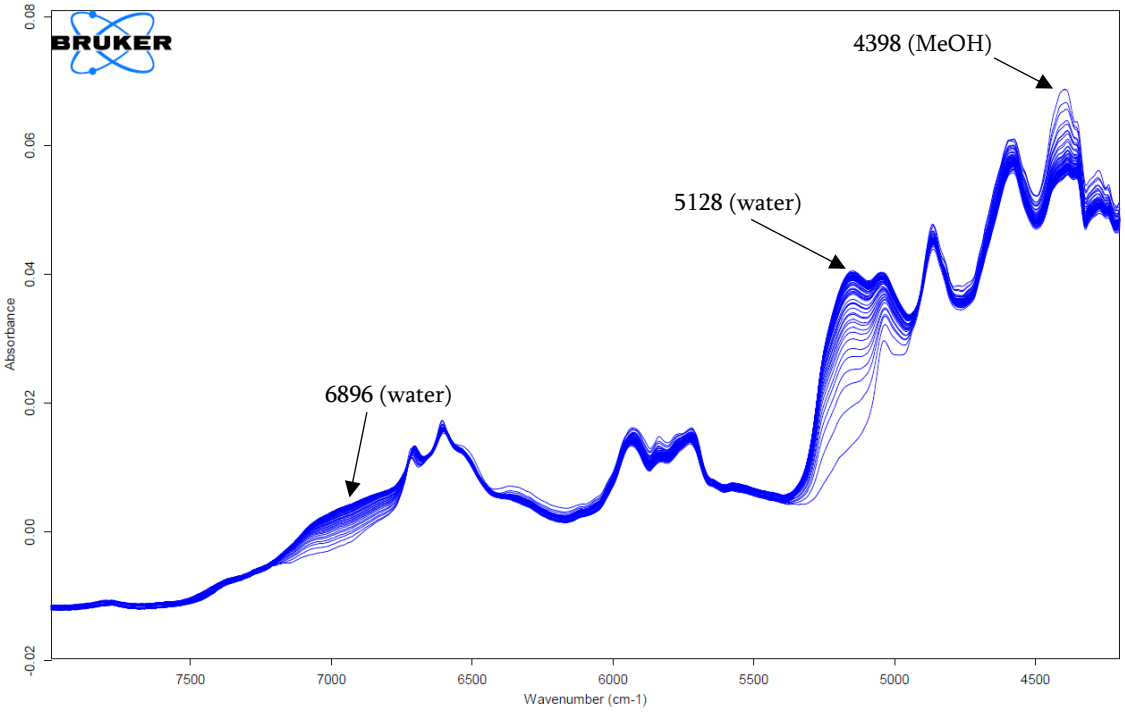

Figure 43. NIR spectra simultaneous static drying

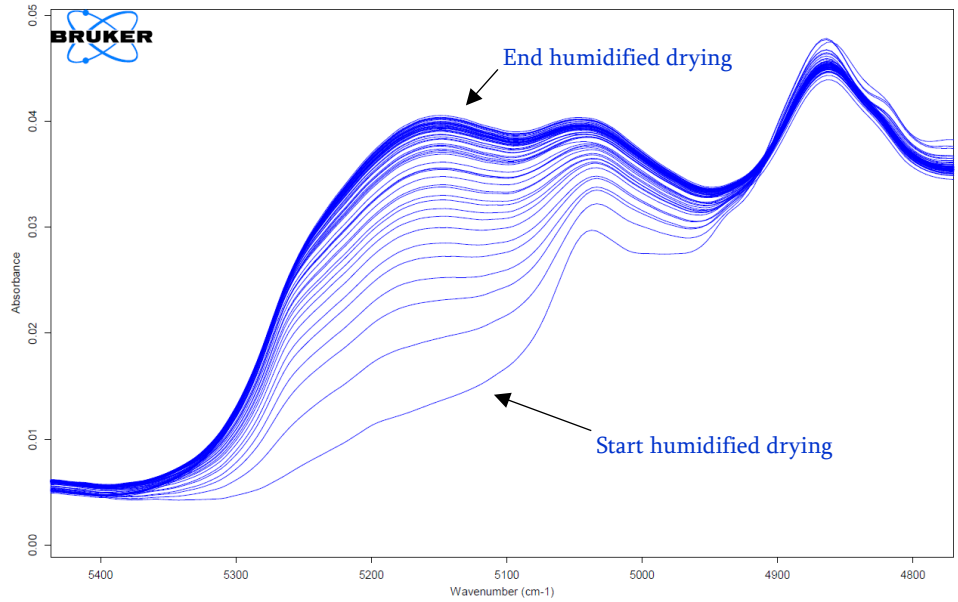

Figure 44. NIR spectra (detail) water sorption region 5128 cm^{-1} simultaneous static drying

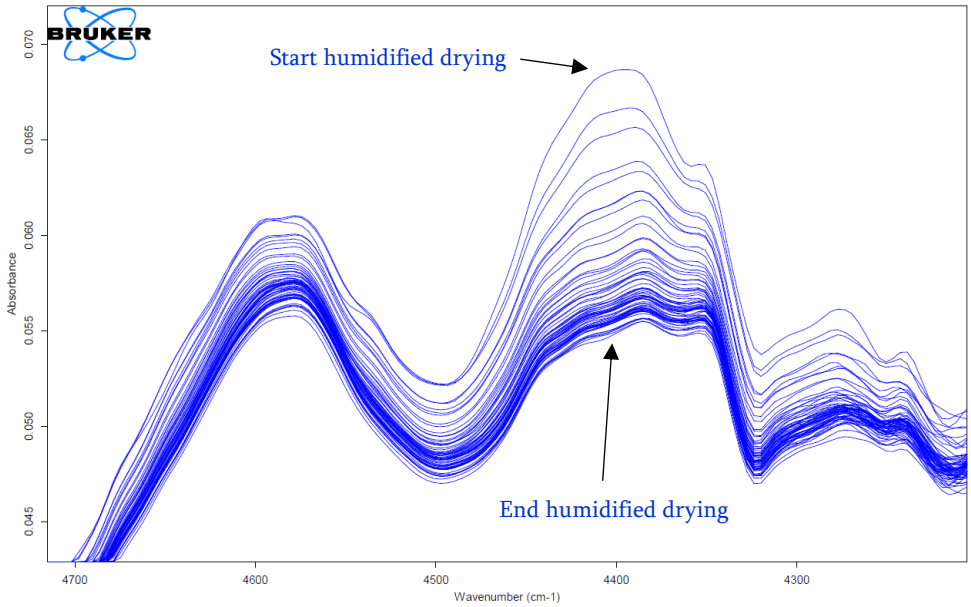

Figure 45. NIR spectra (detail) MeOH sorption region 4398 cm^{-1} simultaneous static drying

Figure 46 shows the result of the water model. Here it was visible that the water uptake occurred faster at the beginning of the process since the difference in water activity between the sample and the humidified nitrogen was greater at this point. As the process approached equilibrium, the water uptake rate decreased. Comparing both experiments, it was apparent that the uptake was more rapid in the first experiment. Besides the fact that it was done in two steps, the relative humidity of this nitrogen flow was higher compared to the one in the simultaneous experiment. The values were 87% RH and 48% RH respectively. This indicated that the water uptake rate was higher as the relative humidity was greater, and thus more water molecules were available. For confirmation of this statement, a third experiment was carried out. The parameters used were identical to those of the simultaneous experiment, except that a nitrogen flow with a relative humidity of 27.5% was used instead of 48%. Figure 46 shows the results of this experiment.

The water uptake rate was also influenced by the flow rate of the nitrogen. In general, it could be said that a higher flow rate and therefore a higher supply of humidified nitrogen would increase the water uptake rate. However, this effect was not apparent in these experiments since, in addition to the flow and RH, the pressure also differed. The conditions of the experiment were respectively 7 nl/min at 200 mbar and 30 nl/min at 950 mbar. Therefore, the actual volumetric flow rate in the oven had to be considered instead of the flow rate at the outlet of the humidifier. The actual volumetric flow rate could be calculated using the ideal gas law and was in this case identical for both experiments.

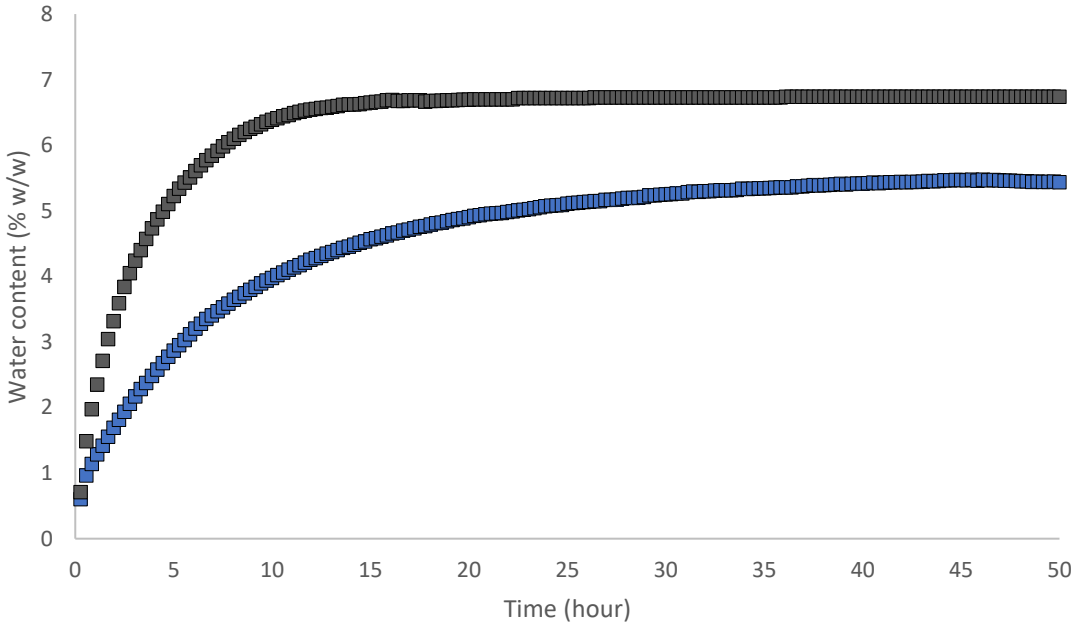

Figure 46. Water content simultaneous static drying at different RH; (black) 48% RH; (blue) 27.5 RH

By comparing both experiments, the previous conclusion was confirmed. Figure 46 demonstrates that the experiment of humidifying at 48% RH (black) resulted in a water content of 5% after 4.5 hours. However, at a RH of 27.5% a water content of 5% was reached after 22.5 hours, which was five times longer. The amount of water supplied at an RH of 48% and a flow of 30 nl/min was approximately 280 mg/min. At a relative humidity of 27.5%, this amount was 160 mg/min. In total, approx. 162 mg of water was adsorbed in each experiment. However, it was important to understand that not all the water entering the oven was in contact with the API because of the volume of the oven (100 l) and a possible bypass of the nitrogen flow.

According to the DVS curve, shown in Figure 30, at 27.5% and 48% relative humidity a water content of 5.6% and 7.5% respectively would be achieved. From Figure 46 it could be concluded that an expected value of 5.5% was obtained. For the experiment at 48% RH, a value of 6.5% was reached. This value had probably not reached equilibrium yet either. The GCHS results showed that the MeOH concentrations after drying in the three experiments are below 500 ppm, which was within the permitted value of the ICH guidelines. For MeOH, this permissible ICH value was 3000 ppm.

4.5 Influence of a solvent change

The analysis of the crystals from the final samples after previous drying experiments showed poor results in terms of the quality of the crystals (cracks and holes). This could be due to several reasons, one of which was the influence of the wash solvent. To confirm whether the choice of solvent was the cause of this problem, the following experiment was performed. A sample after crystallisation was washed with first a mixture of MeOH-water (35-65% v/v). In the second and final washing step, the solvent was changed between MeOH and IPA. The results of the microscope analysis of both samples are shown in Figure 47.

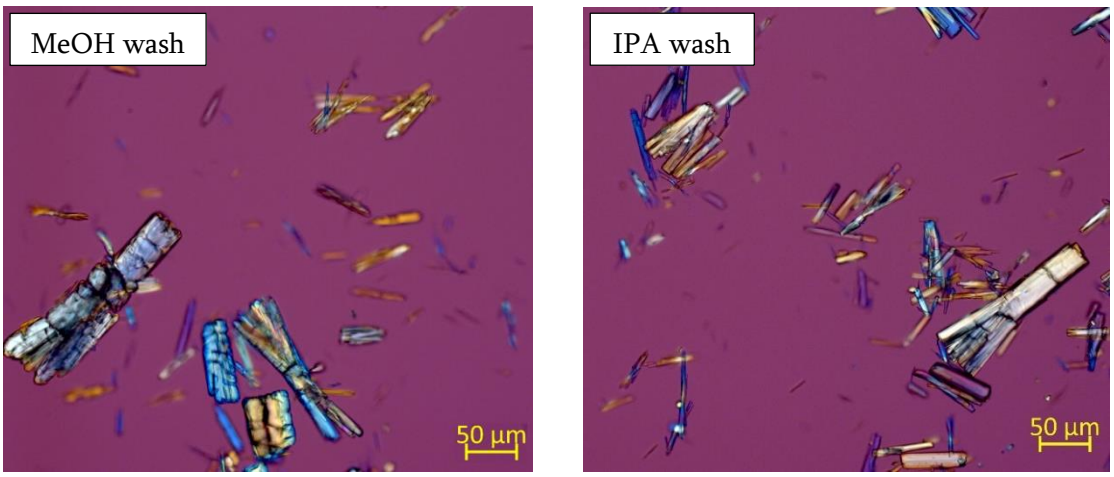

Figure 47. Microscope result compound A after MeOH wash (left) and IPA wash (right)

As shown in Figure 47, the crystals were damaged after the MeOH wash but not after the IPA wash. These cracks reduced the quality of the crystals, which was not desirable for the final product. However, it was visible that the crystals keep their shape, but these cracks reduced the strength of the crystals, which could result in particle breaking in subsequent processes. A clearer representation of the crystals is shown in the results of the SEM analysis in Figure 48 & Figure 49.

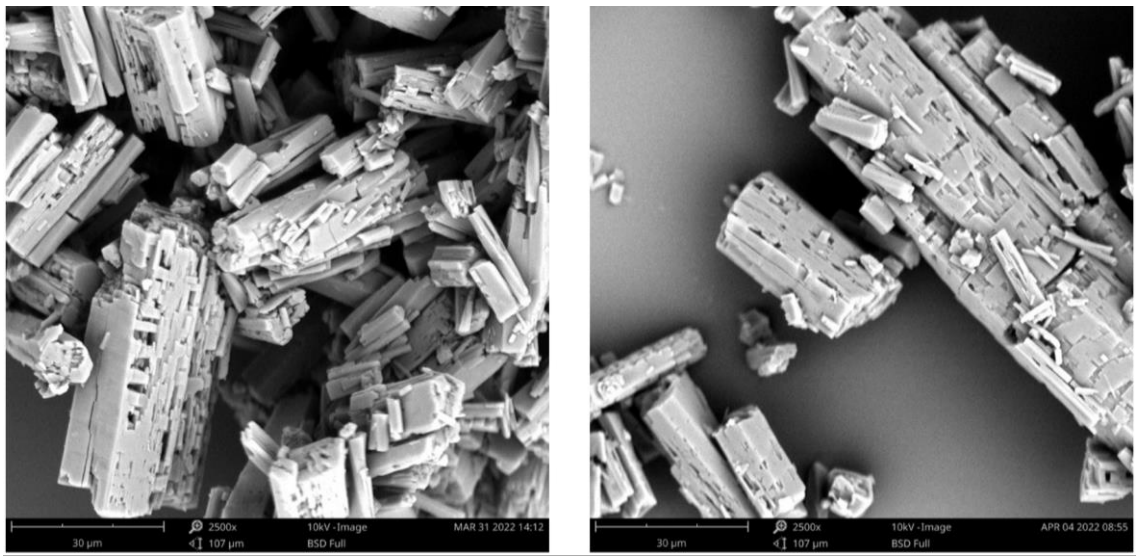

Figure 48. SEM results compound A after MeOH wash (2500x)

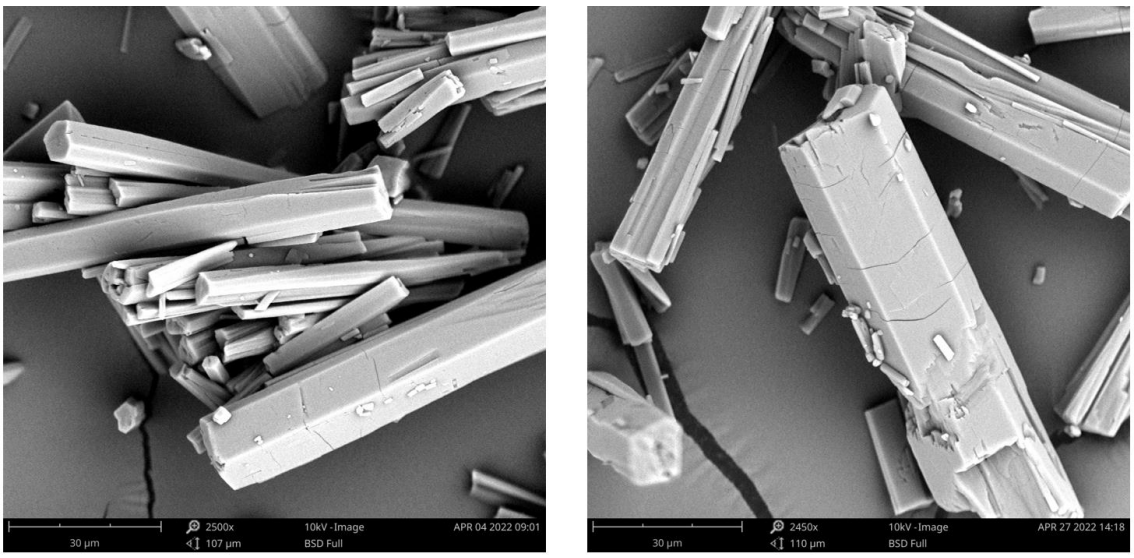

Figure 49. SEM results compound A after IPA wash (2500x)

The SEM results confirmed the previously obtained observation. Also here, clear cracks and even holes were visible in the crystals washed with MeOH. A possible explanation for this damage was the effect of MeOH on the water content of the API. It seemed that MeOH had caused an extraction of water from the crystal structure. This partially removed the strongly bound water, which affected the stability of the crystals. Moreover, this effect took place in a few seconds, which could also contribute to the formation of cracks. If the water extraction was spread over a longer period, it could be possible that the crystals were less damaged. Washing the crystals twice with the MeOH-water mixture resulted in undamaged crystals due to the presence of water in the wash mixture. Because of this, MeOH did not have the same effect as when pure MeOH was used. In the result of the IPA wash, it was clear that this damage was not present. IPA extracted less bound water from the crystal structure so that stability remained unchanged. The fact that IPA extracted less water compared to MeOH could be the result of various reasons. A first possible cause was the mobility of the solvent molecules. The kinetic diameters of IPA, MeOH and water are 4.7 Å, 3.6 Å and 2.6 Å, respectively [50]. In other words, water has the smallest kinetic diameter of the solvents used, which could indicate a more mobile behaviour of water in the crystal structure. Possibly, water was bound at sites that IPA could not reach due to its larger kinetic diameter. In addition to the mobility of the molecules, the affinity of the API to the solvent could also have played a role. However, this characteristic was not studied in detail in this thesis.

4.6 Drying process after IPA wash

4.6.1 Static drying

Following the switch of solvent from MeOH to IPA in the final washing step, a static drying experiment was performed to determine whether the drying behaviour differed from that of the previous drying experiments. For this experiment, a sample of compound A after crystallization, washed with a MeOH-water mixture (35/65% v/v) followed by an IPA wash, was used. The conditions of the drying process are shown in Table 5. The drying process was monitored using NIR spectroscopy and the results of the model are shown in Figure 50.

Table 5. Parameters simultaneous drying experiment IPA wash

Flow (nlpm)	30
Temperature (°C)	21
Pressure (mbar)	700
Relative humidity (%)	15
Mass sample (g)	3

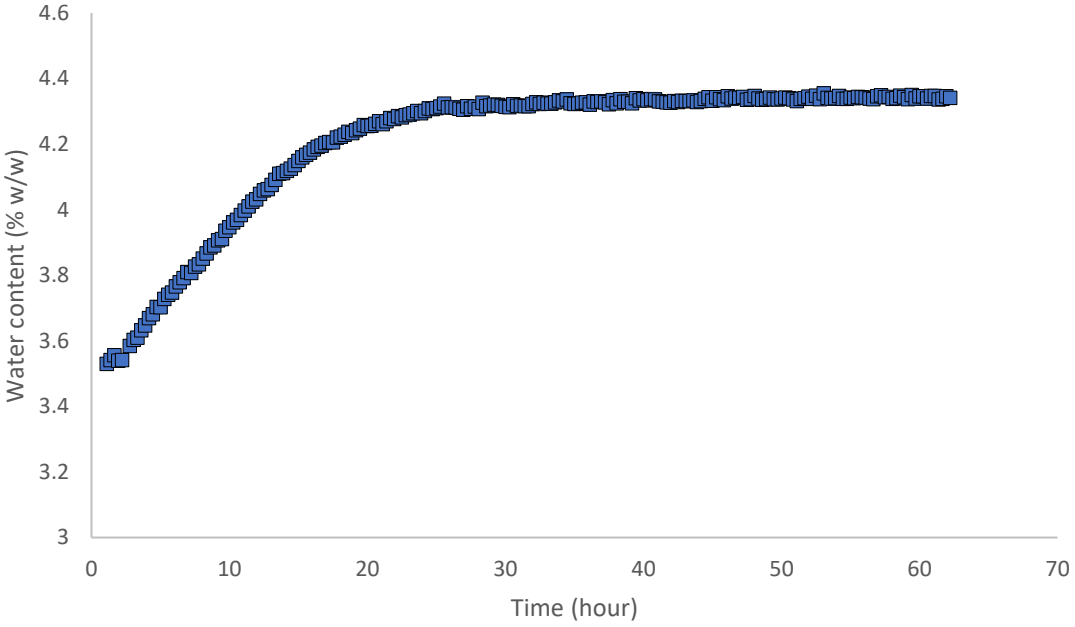

Figure 50. Water content simultaneous static drying IPA wash

In comparison to the drying experiments with MeOH as the final wash solvent, a difference could be noticed from Figure 50 in the initial water content after this washing step. After the IPA wash, 3.1% of water was still present. In contrast, less than 1.0% water was present in the previous drying experiments using MeOH as the final wash solvent. This supported the hypothesis that MeOH extracted water from the crystal structure, causing dehydration of the API. Furthermore, it was apparent that a water content of 4.2% was achieved at a relative humidity of 15%. This result corresponded to the expected value according to the DVS curve, shown in Figure 30. The uptake of 1.2% water required approximately 30 hours. The fact that this adsorption proceeded over a longer period was expected as the relative humidity was only 15%. A comparison between the rate of water adsorption of the sample with the MeOH wash and the sample with the IPA wash could not be made easily, since the relative humidities used in the experiments were different. Given that IPA extracted less water during the washing step, this sample was likely to be less hygroscopic and consequently, the rate of water adsorption was lower.

The drying experiment was conducted for 97 hours in total. The value of IPA measured at the end of the drying process using gas chromatography was 1199 ppm. Although this value was within the ICH guidelines for IPA (5000 ppm), it indicated a more difficult removal of IPA compared to MeOH. This was expected as the boiling point of IPA was higher than that of MeOH, 82.5°C and 64.7°C respectively.

4.6.2 2-step drying vs simultaneous drying

The following drying experiments were conducted in a dynamic dryer to obtain the optimal removal of IPA. Firstly, it was investigated whether there was a difference between a two-step drying process and a simultaneous humidified drying process. The drying conditions of both drying experiments are shown in Table 6. During both drying processes, samples were taken and analysed by GC for the determination of the IPA content. The results are shown in Table 7.

Table 6. Parameters 2-step & simultaneous dynamic drying experiment IPA wash

	2-step drying		simultaneous drying	
	Drying	humidifying	Drying 1	Drying 2
Flow (nlpm)	0.1	1	1	1
Temperature oven (°C)	50	21	50	21
Pressure oven (mbar)	120	700	700	700
Relative humidity (%)	0	25	25	60
mass sample (g)	74.7	74.7	72.2	72.2

Table 7. Results two-step vs simultaneous dynamic drying

Type	Process	Time (hour)	IPA content (%)	Water content (%)
2-step	Start drying	0	10.8	7.8
	Drying	2	4.1	/
	End drying/ start humidifying	4	2.7	1.5
	Humidifying	23	1.2	/
	End humidifying	35	6508 ppm	5.2
Simultaneous	Start humidifying (RH 25%)	0	/	/
	Humidifying (RH 25%)	2	1.7	3.2
	Humidifying (RH 25% to 60%)	4	1.4	4.3
	End humidifying (RH 60%)	13	< 500 ppm	8.3

From Table 7 it was clear that the removal of IPA was faster in the second experiment performed. Comparing the first two hours of both processes, it could be observed that in the first drying experiment, without humidifying, an IPA content of 4.1% was obtained. In the simultaneous drying experiment, after the same time, an IPA content of 1.7% was obtained. The IPA concentration at the beginning of the second experiment was not determined, but it was likely to be approximately the same as in the first experiment. The more rapid decrease in IPA content was mainly due to the use of a nitrogen flow rate 10 times higher in the second experiment compared to the first experiment. This flow ensured a continuous removal of the released IPA. The influence of the relative humidity in this step was difficult to define.

Table 7 also showed that with the two-step drying process after 35 hours of drying, the IPA content was still 6508 ppm and thus not within the ICH guideline of 5000 ppm. As a result, in the simultaneous drying process, an increase of the relative humidity after 4 hours to 60% was carried out. If the final step of both processes were compared, in the first experiment a decrease of approximately 5000 ppm (11536 to 6508 ppm) was visible over a period of 12 hours at a relative humidity of 25%. In the second experiment, a decrease of approximately 13500 ppm (13890 to 500

ppm) was visible over a period of 9 hours at a relative humidity of 60%. This result indicated that IPA removal was faster when using a higher relative humidity since the flow, temperature and pressure were the same. The water content at the end of both drying experiments was 5.1 and 8.3% respectively. These values were in line with the expected values from the DVS curve.

4.6.3 Influence of relative humidity on IPA content

To confirm the influence of relative humidity on IPA content, two more drying experiments were performed. For these experiments, a filter tube was used, in which the humidified nitrogen flow passed through the API. This made the contact surface between the humidified nitrogen flow and the API optimal, resulting in low drying times and thus rapid results. The conditions of both drying experiments are shown in Table 8. Only the relative humidity was changed from 25 to 60%. The solvent contents for IPA and MeOH were determined after each hour using GC. The results are shown in Table 9.

Table 8. Parameters filter tube drying experiment IPA wash

	Test 1	Test 2
Flow (nlpm)	5	5
Temperature (°C)	21	21
Relative humidity (%)	25	60

Table 9. Results filter tube drying experiment IPA wash

	Time (hour)	IPA content (ppm)	MeOH content (ppm)
25% relative humidity	1	8095	937
	2	2050	< 500
60% relative humidity	1	< 500	< 500
	2	< 500	< 500

Table 9 showed a clear difference between the results of both experiments. As expected, the IPA and MeOH removal proceeded more rapidly if a higher relative humidity was used. In the experiment where 25% RH was used, the IPA concentration after one hour was still 8095 ppm (or 8.1%) and after two hours 2050 ppm. In the experiment where 60% RH was used, the IPA content after one hour was already below the detection limit of 500 ppm. In order to minimize drying times and to promote solvent removal, it is therefore recommended to use a higher relative humidity.

For this API, however, a final water content of approximately 5% was desired. This was because of the stability and certain requirements in properties for the product. Since a relative humidity of 60% resulted in a water content of approximately 9%, a drying process with varying relative humidity was desired. In the first part of the drying process, use was made of a nitrogen flow at 60% RH to promote solvent removal. In the second part, a nitrogen flow at 25% RH was used to achieve a water content of 5% in the final product. The following experiment was carried out to determine the time it took for the product to drop in water content to around 5%. The conditions of the drying experiment are shown in Table 10. The filter tube and a nitrogen stream with varying relative humidity were employed. The result is shown in Figure 51.

Table 10. Parameters filter tube drying experiment water content

	Drying 1	Drying 2	Drying 3
Flow (nlpm)	5	5	5
Temperature (°C)	21	21	21
Relative humidity (%)	60	25	15

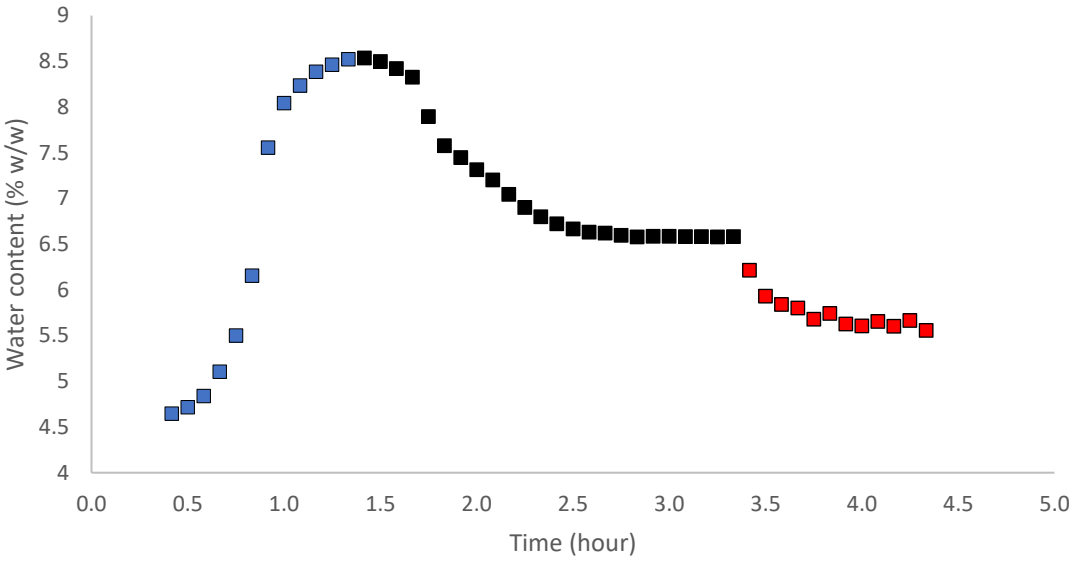

Figure 51. Water content filter tube drying IPA wash; (blue) RH 60%; (black) RH 25%; (red) 15% RH

Figure 51 shows a clear evolution of the water content. First, an RH of 60% was set. Figure 51 shows an increase in the water content to 8.5%. Next, the setpoint was lowered to RH 25%. The water content decreased over a period of approximately one hour to 6.5%. Compared to the DVS curve, shown in Figure 30, this value did not correspond to a relative humidity of 25%. Possibly the RH in the filter tube was higher than the RH specified as the setpoint. To obtain a water content of approximately 5%, the setpoint was lowered to RH 15%. Figure 51 again shows that the water content decreased to 5.4% in about half an hour. From this experiment, it could be concluded that the decrease in water content occurred rapidly in this setup.

The following experiment was carried out to determine the lower limit of relative humidity required during drying. The objective was to determine the level of dehydration in drying conditions without humidified nitrogen and the influence on the crystals. Since, as described in section 4.5, the influence of MeOH could cause water withdrawal resulting in cracks and holes in the crystals, this was checked for dehydration as a result of dry nitrogen. The conditions of this drying experiment are shown in Table 11. The water content, determined by NIR spectroscopy, is shown in Figure 52.

Table 11. Parameters filter tube drying experiment 0% RH

Flow (nlpm)	5
Temperature (°C)	21
Pressure (mbar)	100
Relative humidity (%)	0

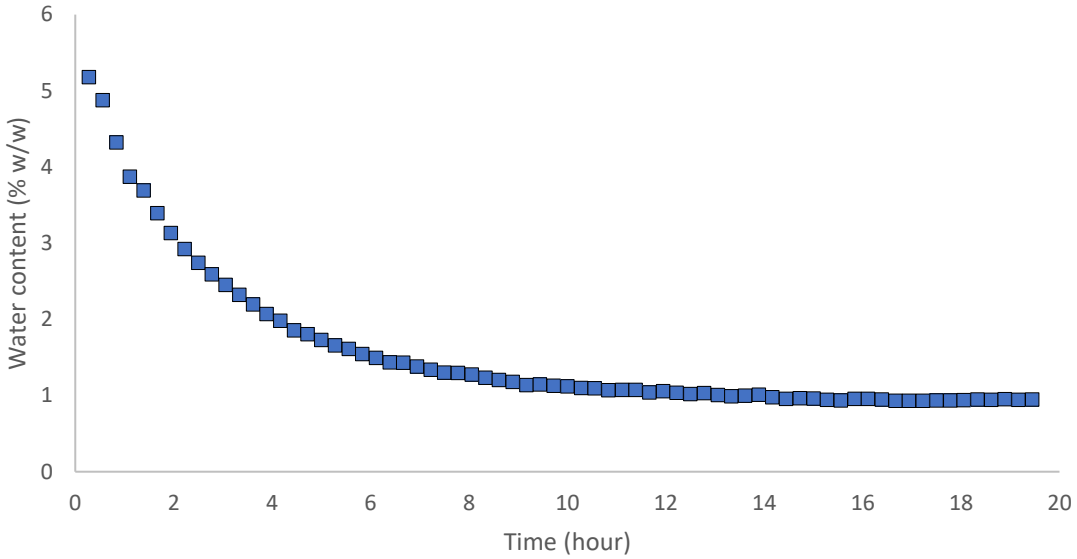

Figure 52. Water content filter drying at 0% RH

As shown in Figure 52, the water content dropped to 0.8%. The remaining water was strongly bound into the crystal structure. Removing this last amount of water would require more extreme conditions than a dry nitrogen flow. The impact of partially dehydrating the compound was analysed using SEM. The results before and after the drying experiment are shown in Figure 53.

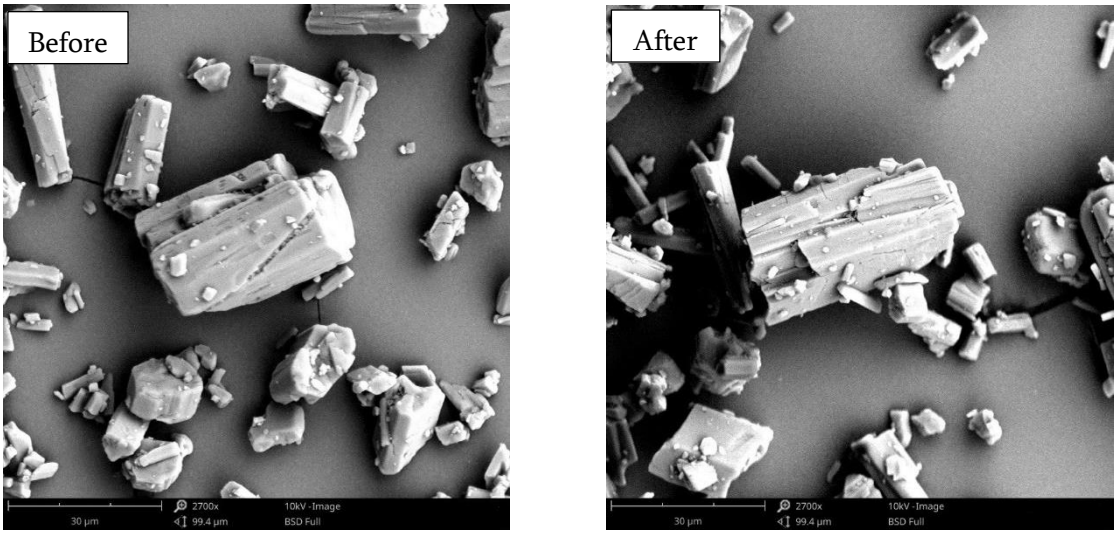

Figure 53. SEM results before (left) & after (right) drying experiment at 0% RH (2700x)

As visible in Figure 53, the crystals were hardly affected by this drying experiment. If the cause of the cracks and holes shown in Figure 48 was the removal of water, the 0.8% of water still present in this experiment was sufficient to prevent such an effect. In addition, the kinetic effect could be a cause since, in the case of MeOH wash, the water was removed much faster, resulting in high stress on the crystals. From this experiment, it could be concluded that the crystals were not much affected during a drying process without humidified nitrogen at room temperature and a reduced pressure of 100 mbar.

4.7 Cake resistance

4.7.1 Compound A

The conditions of the experiment are shown in Table 12. The vial was measured at the top where the compound was exposed to the humidified nitrogen and at the bottom of the vial, as shown in Figure 54. The results of the water content of the top and bottom of the vial are shown in Figure 55.

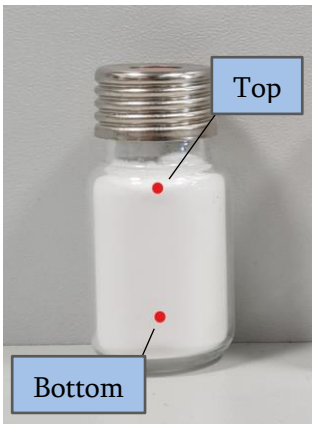

Figure 54. Positioning NIR probe measured at top and bottom

Table 12. Parameters experiment influence of cake resistance

Flow (nlpm)	30
Temperature (°C)	21
Pressure (mbar)	750
Relative humidity (%)	40

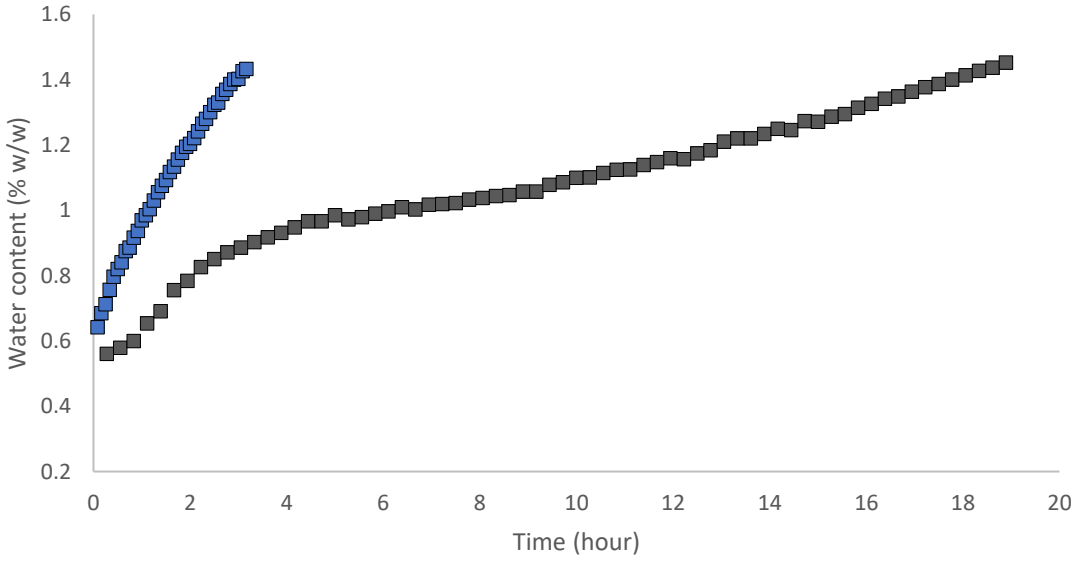

Figure 55. Water content influence of cake resistance; (blue) Top; (black) Bottom

From Figure 55 it could be concluded that the water adsorption was much slower of the compound at the bottom of the vial compared to the top. An increase of approximately 1% took 3 hours at the top and 21 hours at the bottom, which was 7 times longer. The explanation for this was that it was more difficult for the humidified air to reach the bottom of a cake. Therefore, it is important that with static drying, the API is well distributed across the trays in order to increase the contact surface. In industry, it is usually necessary to dry homogeneously, which is why dynamic drying is preferred to static drying.

4.7.2 Compound B

The effect of the cake resistance was also found in the process data of compound B. Figure 56 shows a zoomed in part of the trend of the drying process. The red curve is the speed of the agitator (in rpm) and the green curve refers back to the relative humidity in the outlet stream of the dryer (in %). The set point of the relative humidity was 50% and remained constant during this part.

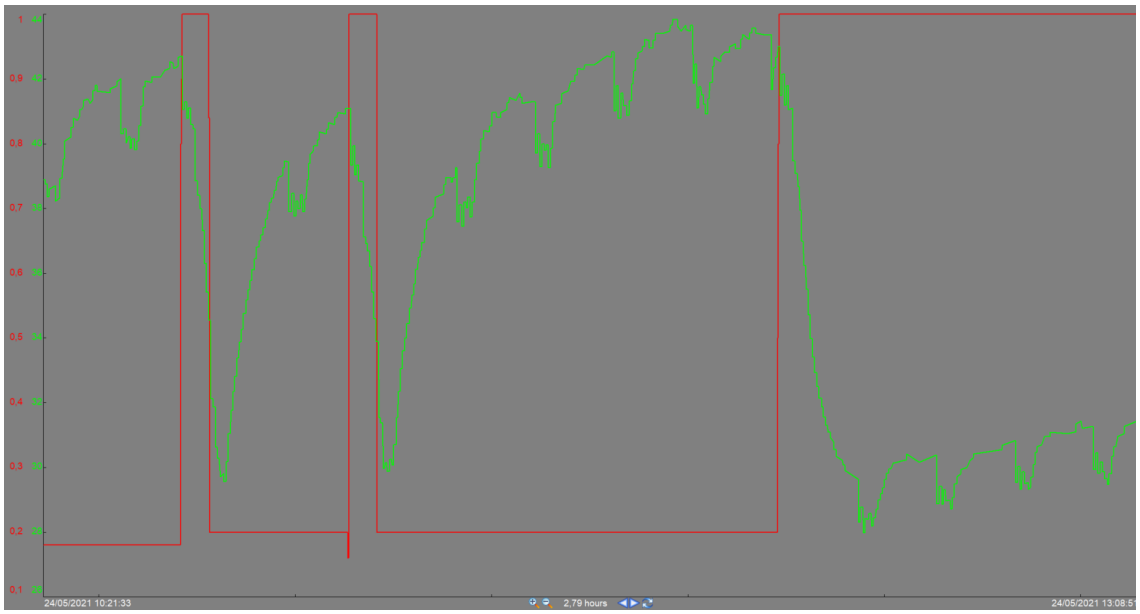

Figure 56. Trend drying compound B influence of the agitator; (Red) RPM agitator; (Green) RH outlet (%)

Figure 56 revealed that the relative humidity at the outlet of the dryer was not constant. Slight drops were visible across the complete trend. The outlet stream of the dryer was connected to a dust filter. In order to prevent the dust filter from clogging, a nitrogen pulse was used. This pulse briefly blew nitrogen over the dust filter every 12 minutes, returning the powder to the dryer. These nitrogen pulses resulted in the small drops in relative humidity. In addition to these slight drops, three great drops were apparent. These drops were a consequence of activating the agitator (shown in red). When no agitation took place, the water exchange occurred mainly in the top layer of the powder. As shown in the experiment above with compound A, the water exchange at the bottom of the powder proceeded at a lower rate than at the top of the powder. In the case compound B was agitated, a drop in the RH of approximately 10% was visible. The reason for this was, because of the agitation, all the powder came in contact with the water molecules present in the dryer. As a result, more water was adsorbed and therefore less water molecules remained in the dryer leading to a drop in RH measurements. In the first two drops, the relative humidity returned rapidly to the initial value since agitation took place for a short period of time. In the last case, agitation occurred for a longer duration and consequently, the relative humidity did not return directly to the original value.

4.8 Humidifier characterisation

4.8.1 Lab humidifier compound A

The characterization of the humidifier was of great importance. The reason being that the relative humidity at the output of the humidifier could differ from the relative humidity present in the dryer. As it was not always possible to measure the relative humidity in the dryer, it was essential to understand and be able to predict the impact on the relative humidity. This characterization was achieved using the humidifier-vacuum oven setup. As a result, the oven could be simultaneously characterized. As mentioned above, the relative humidity depended greatly on both temperature and pressure. In summary, the relative humidity decreases as the temperature increases since warm air can contain more water. If the pressure is reduced, there will be more space for the water molecules and consequently, the relative humidity will decrease as well.

To characterize this setup, it was required to understand what happened during the humidification process. The humidifier was connected to a water source and a nitrogen supply with a regulated pressure of up to 3 bar. The humidifier was operated through the setting of a set point for the outgoing flow and the relative humidity. Additionally, the temperature could be controlled, but this was not included in this study. The nitrogen flow was humidified with the aid of a membrane, which could heat up depending on the quantity of flow to be humidified. The oven was connected to the central vacuum line, through which the nitrogen flow was led away. The minimum pressure the oven could achieve depends on the nitrogen flow directed into the oven. The influence of this flow on the vacuum capacity is shown in Table 13. In this experiment, the pressure of the oven was set as 'Low', which means that the oven was going to achieve the lowest possible pressure.

Table 13. Influence flow on vacuum capacity

SP Pressure (mbar)	Pressure (mbar)	Flow (nl/min)
Low	164	0
Low	224	5
Low	279	10
Low	344	15
Low	411	20
Low	483	25
Low	629	35
Low	800	50

As indicated in Table 13, the minimum pressure the oven could attain without the use of a nitrogen flow was 164 mbar. An increase in the flow resulted in an increase in pressure. A flow of 15 nl/min resulted in an increase in pressure of more than twice the minimum pressure capacity of the oven. At the maximum flow of the humidifier (50 l/min), the oven could only achieve 800 mbar. This posed a problem if a high vacuum was desired. Therefore, the flow should be set low enough to achieve this pressure. But ideally, the flow must also be high enough to allow the nitrogen in the oven to be exchanged sufficiently.

During the performance of the characterization, a frequent discrepancy between the relative humidity measured in the oven and the one measured inside the oven was noticed. The cause was not always clear, but they could all be traced back to a variation in pressure or temperature. A primary cause was a pressure drop between the humidifier output and the oven since the oven was

capable of operating at reduced pressure. As a result, the relative humidity measured in the oven was also lower. In addition to the pressure drop caused by the oven pressure itself, the tubing between the humidifier and the oven was another cause of a pressure drop.

Several properties of the tubing were significant in this context. Firstly, the diameter of the tubing. With a larger diameter tube, the relative humidity was higher compared to a tube with a smaller diameter. This could be explained by the pressure difference between the output of the humidifier and the oven. If the flow had to pass through a small diameter, a higher pressure was needed, resulting in a pressure drop in the oven. Since the pressure decreased, the relative humidity in the dryer reduced as well. In the case of a larger diameter tube, the pressure drop was either low or non-existent. Therefore, the relative humidity was not affected substantially. In addition to the diameter, the length of the tubing had an impact as well. The explanation was identical to that of the diameter. A longer tube required a higher pressure at the output of the humidifier and thus resulting in a pressure difference. A longer tube, therefore, had a similar effect as a smaller diameter and thus caused a reduction of the relative humidity in the dryer. In this study, this was discovered because when using a long tube with a diameter of 6 mm, the set point of 60% RH could not be reached. However, when this tube was replaced with a shorter tube with a diameter of 12 mm, the setpoint of 60% was even exceeded. The effect of the diameter and length of the tubing was mainly a challenge at high flows. When a low flow was used, there were fewer particles per time unit that had to pass through the tubing, which meant there was enough available space for all these particles. However, above a certain flow, the number of particles per time unit exceeded the available space, causing a pressure build-up at the outlet of the humidifier.

The pressure drop in a pipe could be calculated using the Darcy-Weisbach equation, shown in equation 2. Here the relation between the pressure drop, the density of the medium, the diameter and length of the pipe, the flow velocity and the Darcy friction factor is shown. As illustrated in equation 2, a higher value for the length of the pipe results in an increase in pressure drop. Consequently, the pressure at the inlet of the pipe must be higher to reach the desired outlet pressure. The same effect occurs if the diameter value decreases. Lastly, the impact of the flow rate is reflected in this equation. The higher the flow rate, the greater the pressure drop and thus the pressure required at the inlet of the pipe.

$$\frac{\Delta p}{L} = f_D * \frac{\rho}{2} * \frac{(v)^2}{D_H} \qquad (2)$$

In addition to the pressure difference, the length of the tubing had another impact. If a longer tube was used, there was more time for the flow to decrease in temperature before it reached the oven. This temperature reduction would result in an increase in relative humidity with a potential risk of condensation in the tubing. The use of insulated or heated tubing could be a solution to this problem. Along with a pressure drop, the temperature of the humidifier and thus the outlet flow were the most important influences. The reason for this was the heating of the membrane in the humidifier, which occurred as a result of various conditions. With identical flow and pressure, an increase of the setpoint of the relative humidity caused heating in the membrane. As a higher relative humidity was required, the nitrogen flow required more humidification and therefore the membrane heated up. Because the oven temperature in these experiments was always at room temperature, the decrease in temperature between the outlet and the oven caused an increase in relative humidity. This is visible in the results shown in Table 14. For the relative humidity, two values are given. RH

SP is the value of the setpoint adjusted on the humidifier and RH is the relative humidity measured with an RH probe in the oven.

Table 14. Influence RH setpoint on the temperature of the membrane

Oven				Humidifier		
T (°C)	P SP (mbar)	P (mbar)	RH (%)	RH SP (%)	Flow (nlpm)	T membrane (°C)
21.5	900	957	28.5	25	25	28.8
21.5	900	960	54.5	40	25	37.6
21.5	900	966	97.4	60	25	47.5
21.5	700	760	13.8	15	30	18.6
21.5	700	760	30.0	30	30	22.4
21.5	700	760	52.0	40	30	33.5

4.8.2 Compound B

The process data of the drying process of compound B also revealed a difference between the relative humidity at the inlet of the dryer and the RH at the outlet. Figure 57 shows the process data of the drying process of compound B. The flow of the humidifier was 500 nl/min and drying was performed at a reduced pressure of 700 mbar.

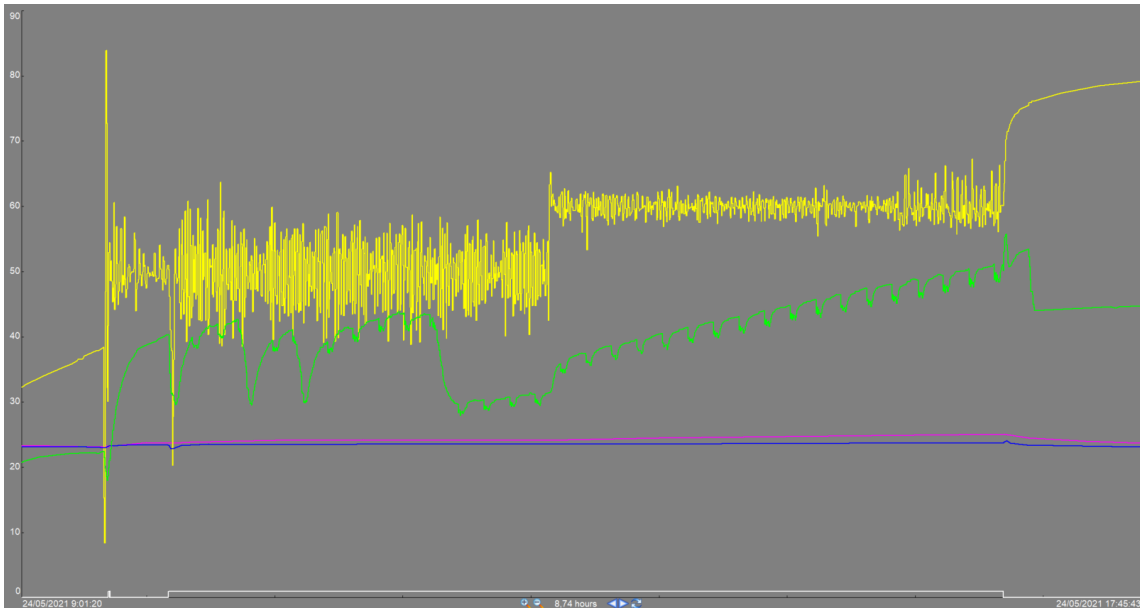

Figure 57. Trend drying compound B variation RH inlet and RH outlet; (Yellow) RH inlet (%); (Green) RH outlet (%); (Pink) Temperature inlet (°C); (blue) Temperature outlet (°C; (White) Vacuum pump (ON/OFF)

From Figure 57 it was apparent that the relative humidity at the inlet of the dryer (yellow) fluctuated. These values indicated the difficulty the humidifier experienced in providing a constant value. This effect was also observed in the humidifier used in the lab with compound A. Furthermore, the relative humidity at the inlet of the dryer (yellow) was higher than that at the outlet of the dryer (green). The RH of the humidifier was set to 50% for the first half of the drying

process followed by 60%. This value was based on the measurement at the outlet of the dryer, as the target value was 50%. The reduced RH measured at the outlet of the dryer could have several causes. Firstly, drying was performed at a reduced pressure of 700 mbar. As described in section 4.8.1, a reduction in pressure also resulted in a reduction in relative humidity. The change in temperature was in this case not an explanation as the temperature measured at the inlet (pink) was higher than the temperature measured at the outlet of the dryer (blue). A decrease in temperature would result in an increase in RH, which was not the case in this situation. Finally, the API itself had the greatest effect on the relative humidity. Since compound B was a channel hydrate and therefore adsorbed water, less water molecules were present in the outlet compared to the inlet of the dryer.

Chapter 5. Conclusions

The use of in-line near-infrared spectroscopy during the humidified drying process was investigated. A successful model was obtained for the determination of the water content from the collected spectra. This model was based on the intensity of the peaks in the regions from 7500 to 6100 cm-1 and from 5452 to 4600 cm-1. A model for the quantification of the solvent content was not constructed since the detection limit was not sufficient for the area of interest of this study. In addition to the in-line NIR spectroscopy application, a distinct view of the water sorption at different relative humidities was achieved using vapor sorption analysis. Compound A was able to adsorb water up to a water content of 11% at a relative humidity of 100%. Furthermore, it became apparent that at low water contents, it became more difficult for the water molecules to leave the crystal. This information was essential since a water content of 5% was targeted for the final product because of its influence on the physicochemical properties. The DVS curve indicated that a water content of 5% is achieved at a relative humidity of approximately 25%.

Next, the influence of ambient air on the water content of a sample was analysed. The effect of direct contact with the ambient air, in the headspace of a closed vial and the combination of the two, was investigated. The exchange of water between the API and the air over the sample depended on the water activity of the product and the relative humidity of the air considered. The higher the difference between both, the higher the rate of water exchange. In case both values were identical, no exchange took place since an equilibrium was already achieved. The headspace in a closed vial had little or no influence on the water content of the sample for various API/Headspace ratios. The ambient air could be considered an infinitely large headspace that will not be altered by the sample. This is similar to a DVS analysis whereby a certain % RH is kept over the sample. So a sample open to the ambient air, will go to an equilibrium water content as shown by the DVS. Furthermore, it was evident that the combination of the headspace in a closed vial and the exposure of the sample to the air in the room had an effect on the water content. By opening the vial a number of times for one minute, the air in the headspace of the vial was renewed, resulting in new available water for exchange. In addition, a difference in the state of the API was also noticed. A distinction was made between a methanol solvate and a hydrate, both containing approximately 1% water at the start. The water exchange rate of the MeOH solvate was considerably lower than that of the hydrate. The MeOH molecules present in the product occupied the positions where water could be adsorbed. Consequently, they had to be displaced first, resulting in a lower exchange rate of water with the API. In general, when the water content needs to be analysed, it is therefore important that this is done before other analyses to minimize contact with the ambient air and to achieve a correct representative result. In addition, the headspace in a vial should be minimised.

Moreover, drying experiments were performed after a MeOH wash and after an IPA wash. This change of solvent used in the final washing step was a result of cracks and holes visible in the crystals after the MeOH wash. The cause of this damage to the crystals was the fact that MeOH extracts water from the crystals, which partially removed the strongly bound water and consequently affected the stability of the crystals. The use of IPA as the final washing step resulted in undamaged crystals, as IPA extracted much less water compared to MeOH. After the IPA wash, 3.1% of water was still present, as opposed to less than 1.0% water present after the MeOH wash. The drying experiments after the MeOH wash indicated that the presence of water molecules during drying promoted the removal of unwanted residual solvent. The water molecules displaced the solvent molecules, causing them to be removed from the crystal structure more readily. In addition, the rate of water adsorption during the drying process was found to be higher when using a higher relative

humidity. In this example, using an RH of 48% resulted in an adsorption rate six times higher compared to using an RH of 28%.

From the drying experiments after the IPA wash, several conclusions were drawn. Firstly, the rate of removal of IPA was found to be lower than that of MeOH. Secondly, a higher nitrogen flow indicated an improved removal of IPA, as this flow ensures the removal of released solvent molecules. Furthermore, it became apparent that the use of a higher relative humidity resulted in a more rapid removal of the unwanted IPA molecules. A 5000 ppm decrease over a 12 hour time period was observed at 25% RH as opposed to a 13500 ppm decrease over a 9 hour time period at 60% RH. Lastly, it was found that the crystals did not experience adverse effects during drying at a relative humidity of 0%. The slow kinetics of this water removal, down to 0.8% water, ensured that no cracks or holes were formed in the crystals compared to the effect of the MeOH wash. Ultimately, a drying process was drawn up for component A consisting of a drying step at 60% RH to achieve the removal of IPA (below 5000 ppm), followed by a drying step at 25% RH to achieve the desired water content of 5% for the final product.

In this study, an image of the behaviour of water exchange between compound A and the ambient air was obtained using a vapor sorption analyser. However, the behaviour of compound A towards the washing solvents, MeOH and IPA, is not completely known. From the experiments preformed in this thesis, it could be concluded that a solvate was formed with both washing solvents. To obtain a complete understanding of the behaviour regarding these washing solvents, a vapor sorption isotherm can be obtained with the help of a vapor sorption analyser, which is able to work with MeOH and IPA. In addition, a drying process for compound A was successfully created in this study. In the future, the upscaling of this drying process should be monitored and further optimised to the drying equipment available.

In addition to the drying experiments, the influence of the ambient air, directly and in the headspace of a vial, on compound A was analysed. It appeared evident that after closing the vial, the water content of the sample continued to change due to the presence of a headspace. An additional experiment can be performed to confirm the importance of no headspace for an accurate water content analysis. By exposing a completely filled vial (no headspace) to the ambient air a number of times, the water content should not be greatly affected. Furthermore, it is important to note that the influence of the ambient air depends greatly on the sample itself. Both the type of hydrate/solvate and the state in which the sample is located (such as solvent content). This influence should therefore be examined individually for each API, if such information is required.

References

[1] K. Stone, “api-active-pharmaceutical-ingredient-2663020,” 2021. https://www.verywellhealth.com/api-active-pharmaceutical-ingredient-2663020 (accessed Mar. 10, 2022).

[2] J. Lu and S. Rohani, “Polymorphism and Crystallization of Active Pharmaceutical Ingredients (APIs),” *Current Medicinal Chemistry*, vol. 16, no. 7, pp. 884–905, Mar. 2009, doi: 10.2174/092986709787549299.

[3] E. Tieger *et al.*, “Studies on the crystal structure and arrangement of water in sitagliptin l-tartrate hydrates,” *CrystEngComm*, vol. 18, no. 21, pp. 3819–3831, 2016, doi: 10.1039/c6ce00322b.

[4] E. Jurczak, A. H. Mazurek, Ł. Szeleszczuk, D. M. Pisklak, and M. Zielińska-Pisklak, “Pharmaceutical hydrates analysis—overview of methods and recent advances,” *Pharmaceutics*, vol. 12, no. 10, pp. 1–25, Oct. 2020, doi: 10.3390/pharmaceutics12100959.

[5] S. R. Vippagunta, H. G. Brittain, and D. J. W. Grant, “Crystalline solids,” *Advanced Drug Delivery Reviews*, vol. 48, pp. 3–26, 2001, doi: https://doi.org/10.1016/S0169-409X(01)00097-7.

[6] D. Chen and R. Suryanarayanan, “HYGROSCOPICITY OF PHARMACEUTICAL CRYSTALS,” vol. 293, Jan. 2009.

[7] T. A. Watts, S. M. Niederberger, and J. A. Swift, “Improving Channel Hydrate Stability via Localized Chemical Tuning of the Water Environment,” *Crystal Growth and Design*, vol. 21, no. 9, pp. 5206–5214, Sep. 2021, doi: 10.1021/acs.cgd.1c00551.

[8] R. Mizoguchi and H. Uekusa, “Elucidation of the crystal structures and dehydration behaviors of ondansetron salts,” *Crystals (Basel)*, vol. 9, no. 3, Mar. 2019, doi: 10.3390/cryst9030180.

[9] J. Burgbacher and J. Wiss, “Industrial applications of online monitoring of drying processes of drug substances using NIR,” *Organic Process Research and Development*, vol. 12, no. 2, pp. 235–242, Mar. 2008, doi: 10.1021/op700293p.

[10] P. Grobelny, A. Mukherjee, and G. R. Desiraju, “Polymorphs and hydrates of Etoricoxib, a selective COX-2 inhibitor,” *CrystEngComm*, vol. 14, no. 18, pp. 5785–5794, Sep. 2012, doi: 10.1039/c2ce06604a.

[11] G. X. Zhou, J. Dorwart, B. Izzo, J. Kukura, G. Bicker, and J. Wyvratt, “Determination and Differentiation of Surface and Bound Water in Drug Substances by Near Infrared Spectroscopy,” *J Pharm Sci*, vol. 92, pp. 1058–1065, 2003.

[12] M. Preskar, K. Korasa, T. Vrbanec, D. Klement, F. Vrečer, and M. Gašperlin, “Applicability of Raman and near-infrared spectroscopy in the monitoring of freeze-drying injectable ibuprofen,” *Drug Development and Industrial Pharmacy*, vol. 47, no. 5, pp. 758–769, 2021, doi: 10.1080/03639045.2021.1934864.

[13] S. L. Shamblin, B. C. Hancock, and G. Zografi, “Water vapor sorption by peptides, proteins and their formulations,” *European Journal of Pharmaceutics and Biopharmaceutics*, vol. 45, no. 3, pp. 239–247, 1998, doi: 10.1016/S0939-6411(98)00006-X.

[14] L. Chablani, M. K. Taylor, A. Mehrotra, P. Rameas, and W. C. Stagner, “Inline real-time near-infrared granule moisture measurements of a continuous granulation-drying-milling process,” *AAPS PharmSciTech*, vol. 12, no. 4, pp. 1050–1055, Dec. 2011, doi: 10.1208/s12249-011-9669-z.

[15] W. Cao, C. Mao, W. Chen, H. Lin, S. Krishnan, and N. Cauchon, “Differentiation and quantitative determination of surface and hydrate water in lyophilized mannitol using NIR spectroscopy,” *Journal of Pharmaceutical Sciences*, vol. 95, no. 9, pp. 2077–2086, 2006, doi: 10.1002/jps.20706.

[16] T. Amira, P. Roman, and Z. Fethi, “On-line monitoring of vacuum drying of theophylline using NIR spectroscopy: solid-state transitions, water content and semi-empirical modeling,” *Drug Development and Industrial Pharmacy*, vol. 42, no. 11, pp. 1825–1832, Nov. 2016, doi: 10.1080/03639045.2016.1178768.

[17] E. Yonemochi and H. Uekusa, “Pharmaceutical Crystals,” *MDPI*, vol. 141, 2020, [Online]. Available: www.mdpi.com/journal/crystals

[18] D. S. Hsieh, Q. Gao, M. Huang, L. M. Dimemmo, M. Lindrud, and T. Razler, “From Drying Kinetics, Solvate Structure, Particle Morphology, and Modeling to Optimal Drying Protocol,” *Organic Process Research and Development*, vol. 21, no. 10, pp. 1509–1520, Oct. 2017, doi: 10.1021/acs.oprd.7b00162.

[19] I. Ostergaard, H. Lopez de Diego, and H. Qu, “Crystallization of Cephradine Polymorphs and Hydrates from Mixed Solvents of Methanol and Water,” *Chemical Engineering and Technology*, vol. 42, no. 7, pp. 1512–1518, Jul. 2019, doi: 10.1002/ceat.201800689.

[20] E. W. Conder *et al.*, “The Pharmaceutical Drying Unit Operation: An Industry Perspective on Advancing the Science and Development Approach for Scale-Up and Technology Transfer,” *Organic Process Research and Development*, vol. 21, no. 3, pp. 420–429, Mar. 2017, doi: 10.1021/acs.oprd.6b00406.

[21] G. Zhang, X. Xiao, L. Zhang, G. Ren, and S. Zhang, “Hydrates and Solvates of Acotiamide Hydrochloride: Crystallization, Structure, Stability, and Solubility,” *Crystal Growth and Design*, vol. 19, no. 2, pp. 768–779, Feb. 2019, doi: 10.1021/acs.cgd.8b01360.

[22] D. J. Lamberto and J. Neuhaus, “Robust Process Scale-Up Leveraging Design of Experiments to Map Active Pharmaceutical Ingredient Humid Drying Parameter Space,” *Organic Process Research and Development*, vol. 25, no. 2, pp. 239–249, Feb. 2021, doi: 10.1021/acs.oprd.0c00475.

[23] S. Byrn, R. Pfeiffer, M. Ganey, C. Hoiberg, and G. Poochikian, “Pharmaceutical solids: a strategic approach to regulatory considerations,” *Pharmaceutical Research*, vol. 12, no. 7, pp. 945–954, 1995, doi: 10.1023/A:1016241927429.

[24] S. H. Cypes *et al.*, "Drying an organic monohydrate: Crystal form instabilities and a factory-scale drying scheme to ensure monohydrate preservation," *Organic Process Research and Development*, vol. 8, no. 4, pp. 576–582, Jul. 2004, doi: 10.1021/op049956a.

[25] Parikh Dilip, "SOLIDS DRYING: BASICS AND APPLICATIONS," *Chemical Engineering*, Apr. 01, 2014. https://www.chemengonline.com/solids-drying-basics-and-applications/?printmode=1#disqus_thread (accessed Apr. 10, 2022).

[26] E. Tsotsas, T. Metzger, V. Gnielinski, and E.-U. Schlünder, "Drying of Solid Materials," in *Ullmann's Encyclopedia of Industrial Chemistry*, Wiley-VCH Verlag GmbH & Co. KGaA, 2010. doi: 10.1002/14356007.b02_04.pub2.

[27] H. L. Lim, K. P. Hapgood, and B. Haig, "Understanding and preventing agglomeration in a filter drying process," *Powder Technology*, vol. 300, pp. 146–156, Oct. 2016, doi: 10.1016/j.powtec.2016.03.003.

[28] "Welcome to the ICH Official Website." https://www.ich.org/ (accessed May 01, 2022).

[29] S. Zhang and D. J. Lamberto, "Development of new laboratory tools for assessment of granulation behavior during bulk active pharmaceutical ingredient drying," *Journal of Pharmaceutical Sciences*, vol. 103, no. 1, pp. 152–160, 2014, doi: 10.1002/jps.23762.

[30] D. J. Lamberto, A. Diaz-Santana, and G. Zhou, "Form Conversion and Solvent Entrapment during API Drying," *Organic Process Research and Development*, vol. 21, no. 11, pp. 1828–1834, Nov. 2017, doi: 10.1021/acs.oprd.7b00270.

[31] D. Am Ende, M. Birch, S. J. Brenek, and M. T. Maloney, "Development and application of laboratory tools to predict particle properties upon scale-up in agitated filter-dryers," *Organic Process Research and Development*, vol. 17, no. 10, pp. 1345–1358, Oct. 2013, doi: 10.1021/op400080x.

[32] D. J. Lamberto, B. Cohen, J. Marencic, C. Miranda, R. Petrova, and L. Sierra, "Laboratory methods for assessing API sensitivity to mechanical stress during agitated drying," *Chemical Engineering Science*, vol. 66, no. 17, pp. 3868–3875, Sep. 2011, doi: 10.1016/j.ces.2011.05.016.

[33] C. D. Papageorgiou *et al.*, "Development of a Novel Screening Methodology for the Assessment of the Risk of Particle Size Attrition during Agitated Drying," *Organic Process Research and Development*, vol. 24, no. 2, pp. 242–254, Feb. 2020, doi: 10.1021/acs.oprd.9b00502.

[34] B. Aukema, "Mollier-Diagram." https://www.mollier-diagram.com/ (accessed May 21, 2022).

[35] S. J. Schmidt and J. W. Lee, "Comparison between water vapor sorption isotherms obtained using the new dynamic dewpoint isotherm method and those obtained using the standard saturated salt slurry method," *International Journal of Food Properties*, vol. 15, no. 2, pp. 236–248, Mar. 2012, doi: 10.1080/10942911003778014.

[36] P. Hamilton *et al.*, "Investigation of factors affecting isolation of needle-shaped particles in a vacuum-agitated filter drier through non-invasive measurements by Raman

spectrometry," *Chemical Engineering Science*, vol. 101, pp. 878–885, 2013, doi: 10.1016/j.ces.2013.05.035.

[37] M. Manley, "Near-infrared spectroscopy and hyperspectral imaging: Non-destructive analysis of biological materials," *Chemical Society Reviews*, vol. 43, no. 24, pp. 8200–8214, Dec. 2014, doi: 10.1039/c4cs00062e.

[38] H. Büning-Pfaue, "Analysis of water in food by near infrared spectroscopy," *Food Chemistry*, vol. 82, no. 1, pp. 107–115, 2003, doi: 10.1016/S0308-8146(02)00583-6.

[39] A. M. Demers, R. Gosselin, J. S. Simard, and N. Abatzoglou, "In-line near infrared spectroscopy monitoring of pharmaceutical powder moisture in a fluidised bed dryer: An efficient methodology for chemometric model development," *Canadian Journal of Chemical Engineering*, vol. 90, no. 2, pp. 299–303, Apr. 2012, doi: 10.1002/cjce.20691.

[40] A. Peinado, J. Hammond, and A. Scott, "Development, validation and transfer of a Near Infrared method to determine in-line the end point of a fluidised drying process for commercial production batches of an approved oral solid dose pharmaceutical product," *Journal of Pharmaceutical and Biomedical Analysis*, vol. 54, no. 1, pp. 13–20, Jan. 2011, doi: 10.1016/j.jpba.2010.07.036.

[41] R. L. Green, G. Thurau, N. C. Pixley, A. Mateos, R. A. Reed, and J. P. Higgins, "In-line monitoring of moisture content in fluid bed dryers using near-IR spectroscopy with consideration of sampling effects on method accuracy," *Analytical Chemistry*, vol. 77, no. 14, pp. 4515–4522, Jul. 2005, doi: 10.1021/ac050272q.

[42] S. Maitra and J. Yan, "Principle Component Analysis and Partial Least Squares: Two Dimension Reduction Techniques for Regression," *Casualty Actuarial Society*, vol. 21, pp. 79–90, 2008.

[43] K. R. Rajisha, L. A. Pothan, and Thomas S., "Interface engineering of natural fibre composites," in *Interface Engineering of Natural Fibre Composites for Maximum Performance*, vol. 428, Woodhead Publishing Series in Composites Science and Engineering, 2011, pp. 241–274.

[44] S. N. Ronkart, C. Deroanne, M. Paquot, C. Fougnies, and C. S. Blecker, "Impact of the crystallisation pathway of inulin on its mono-hydrate to hemi-hydrate thermal transition," *Food Chemistry*, vol. 119, no. 1, pp. 317–322, Mar. 2010, doi: 10.1016/j.foodchem.2009.06.035.

[45] A. M. Lawson, "Mass Spectrometry The Fundamental Principles," in *Mass Spectrometry*, vol. 747, A. M. Lawson, Ed. De Gruyter, 1988, pp. 1–52. doi: 10.1515/9783112418123.

[46] "Extreme Solarization Resistant Reflection/Backscatter Probes." https://www.oceaninsight.com/products/fibers-and-probes/probes/reflectionbackscatter-probes/extreme-solarization-resistant-reflectionbackscatter-probes/ (accessed May 16, 2022).

[47] "Principle of Karl Fischer Titration - BYJU'S." https://byjus.com/chemistry/karl-fischer-titration/#:~:text=The%20principle%20of%20Karl%20Fischer,all%20the%20water%20is%20consumed. (accessed May 21, 2022).

[48] "Karl Fischer Titration – Measuring Principle," 2017. https://www.gpsil.co.uk/karl-fischer-titration-measuring-principle/ (accessed May 21, 2022).

[49] C. Invernizzi, T. Rovetta, M. Licchelli, and M. Malagodi, "Mid and near-infrared reflection spectral database of natural organic materials in the cultural heritage field," *International Journal of Analytical Chemistry*, vol. 2018, 2018, doi: 10.1155/2018/7823248.

[50] K. Dedecker, E. Dumas, B. Lavédrine, N. Steunou, and C. Serre, "5 - Metal-organic frameworks for the capture of volatile organic compounds and toxic chemicals," in *Metal-Organic Frameworks (MOFs) for Environmental Applications*, Elsevier, 2019, pp. 141–178. doi: 10.1016/B978-0-12-814633-0.00007-7.

Appendix

A. Overview drying experiments

Table 15. Overview conditions drying experiments

Experiment		Type of dryer	Mass sample (g)	Flow (nlpm)	Temperature (°C)	Pressure (mbar)	Relative humidity (%)
2-step static drying MeOH wash	Drying	static (oven)	3.0	7.0	40	200	0.0
	Humidifying			7.0	21	200	87.0
Simultaneous static drying MeOH wash 48% RH		static (oven)	3.0	30.0	21	950	48.0
Simultaneous static drying MeOH wash 27.5% RH		static (oven)	3.0	30.0	21	950	27.5
Static drying IPA wash		static (oven)	3.0	30.0	21	700	15.0
Influence of cake resistance on water content		static (oven)	/	30.0	21	750	40.0
2-step dynamic drying IPA wash	Drying	Agitated dryer	74.7	0.1	50	120	0.0
	Humidifying			1.0	21	700	25.0
Simultaneous dynamic drying IPA wash	Drying 1	Agitated dryer	72.2	1.0	50	700	25.0
	Drying 2			1.0	21	700	60.0
Filter tube drying 25% RH		Filter dryer	/	5.0	21	/	25.0
Filter tube drying 60% RH		Filter dryer	/	5.0	21	/	60.0
Filter tube drying	Drying 1	Filter dryer	/	5.0	21	/	60.0
	Drying 2		/	5.0	21	/	25.0
	Drying 3		/	5.0	21	/	15.0
Filter rube drying 0% RH		Filter dryer	/	5.0	21	100	0.0